Energy & Buildings 287 (2023) 112998

Contents lists available at ScienceDirect

Energy & Buildings

journal homepage: www.elsevier.com/locate/enb

Overheating analysis of optimized nearly Zero-Energy dwelling during current and future heatwaves coincided with cooling system outage

Ramin Rahif [a,*], Mostafa Kazemi [b], Shady Attia [a]

[a] Sustainable Building Design Lab, Dept. UEE, Faculty of Applied Sciences, University of Liège, Belgium
[b] GeMMe Building Materials, Department of Urban and Environmental Engineering (UEE), Faculty of Applied Sciences, University of Liège, 4000, Liège, Belgium

ARTICLE INFO

Article history:
Received 24 November 2022
Revised 8 March 2023
Accepted 14 March 2023
Available online 18 March 2023

Keywords:
Climate change
Optimization
Residential building
Thermal comfort
HVAC
Final energy use

ABSTRACT

It is expected that heatwaves will strike more frequently and with higher temperatures with the continuation of global warming. More extreme heatwaves concurrent with disruptions in the cooling system can lead to significant overheating problems in buildings affecting occupants' health, productivity, and comfort. This paper projects current and future heatwaves on an optimized nearly Zero-Energy terraced dwelling in Brussels, assuming the outage of the cooling system. Initially, a multi-objective optimization is performed considering 13 passive design strategies using the Genetic Algorithm (GA) based on the Non-dominated Sorting Genetic Algorithm 2 (NSGA-II) method. It is found that high ventilation rate, low infiltration rate, high insulation, high thermal mass, integration of green roof, and application of operable roller blinds are beneficial in reducing the final HVAC energy use up to 32% and enhancing thermal comfort up to 46%. Subsequently, three optimal solutions are selected and analyzed under the highest maximal temperature heatwaves detected during the 2001–2020, 2041–2060, and 2081–2100 periods. It is found that non of the optimal solutions are able to fully suppress overheating during heatwaves and the cooling system outage. The indoor operative temperatures reach more than 29 °C, which can cause serious health issues for the occupants. The situation will be exacerbated in the future since an increase in maximum Heat Index (HI) between 0.28 °C and 0.49 °C, an increase in the maximum operative temperature between 1.34 °C and 2.33 °C, and a decrease in Thermal Autonomy (TA) between 17% and 28% are estimated. Finally, some recommendations are provided for practice and future research.

1. Introduction

1.1. Background

Climate change is the long-term shift in weather patterns due to natural causes (e.g., variations in solar cycles) or human activities (mainly due to the use of fossil fuels). The Intergovernmental Panel on Climate Change (IPCC) Sixth Assessment Report (AR6) [1] predicted that the average global surface temperature will increase between 1 and 5.7 °C by the end of the century. Similarly, the European Environment Agency (EEA) foresees an increase in average air temperature between 2.5 °C and 4 °C by 2071–2100 over Europe. The situation will be worse in cities due to the Urban Heat Island (UHI) effect. According to [2,3], the ambient temperature in cities is 5 °C-10 °C higher compared to the surrounding areas. This undesirable warming can exacerbate existing problems in large cities, such as water scarcity, air pollution, and heatwaves.

Although there is no commonly accepted definition of heatwaves, they are understood to be a period of sweltering weather that can or cannot be accompanied by high humidity levels, usually with an obvious effect on humans or natural systems [4]. Heatwaves usually happen due to the trapped air in a specific region that can last for two or more days during the hot season. As climate change continues to raise global temperatures, the heatwaves start earlier in some places around the world [5]. It is also found that with the continuation of global warming, future heatwaves will tend to be longer and more severe [6]. In late June and July 2019, most European countries experienced consecutive days above 30 °C, and some countries, such as Belgium, France, Germany, the Netherlands, and the UK, set a new all-time high [7]. Such extreme heatwave events can lead to water shortages, blackouts, and overheating problems in buildings [8].

Overheating or accumulation of heat in buildings forfeits occupants' productivity, comfort, and health, which in severe cases can lead to heat exhaustion, dehydration, and heat stroke [9,10]. According to the UK Housing Health and Safety Rating System (HHSRS), indoor temperatures above 25 °C can increase mortality

* Corresponding author.
E-mail address: ramin.rahif@uliege.be (R. Rahif).

https://doi.org/10.1016/j.enbuild.2023.112998
0378-7788/

rates [11]. Over 2500 excess deaths were reported across Europe during the summer 2019 heatwaves [12], of which 716 died in Belgium [13], 1435 in France [14], 400 in the Netherlands [15], 900 in the UK [16], and 500 in Germany [17]. It is urged to optimize and enhance the thermal performance of buildings so that they act as a shelter and keep the occupants safe during hot weather conditions.

Optimization is the procedure of making a design or a system perform as perfectly or most effectively as possible [18]. In other words, it is the process of identifying designs that minimize or maximize a specific goal. Simulation-based optimization is undoubtedly a great approach to reach many design targets, opening a new era for building designers and modellers. Several simulation programs have been introduced in recent decades to perform building optimization, such as DesignBuilder, BuildSimHub, jEPlus + EA, Autodesk Insight, etc. It should be noted that the aim of optimization in Building Performance Simulation (BPS) is not necessarily to find globally optimal solutions to a problem due to the limitations of the simulation program itself [19] or the nature of the problem [20]. The optimization methods and their applications are extensively reviewed in some previous studies [18,20–23].

1.2. Literature review

Several studies have been conducted to optimize the energy efficiency and thermal comfort of buildings in different regions by considering various input factors and employing metaheuristic algorithms. These studies have demonstrated promising results in terms of reducing energy consumption and improving thermal comfort. Chegari et al. [24] optimized a two-floor residential unit in Morocco by considering thermo-physical parameters of the building envelope as the input factor. They aimed at minimizing the computation time via the integration of Artificial Neural Networks (ANN) coupled with multiple metaheuristic algorithms such as Multi-Objective Particle Swarm Optimization (MOPSO), Multi-Objective Genetic Algorithm (MOGA), and Non-dominated Sorting Genetic Algorithm 2 (NSGA-II). They found that the coupling between ANN and MOPSO has the greatest desired performance among others by reducing the total heating and cooling thermal needs by 74.52% while enhancing the indoor thermal comfort (quantified by degree-hours *"Dh"*) by 4.32%. Vukadinović et al. [25] discussed a performed optimization for a detached passive house building in Serbia based on the NSGA-II method. The optimization variables include the parameters of the passive solar design, such as glazing type, window shading, wall construction, and the window-to-wall ratio of each façade individually. Prior to optimization, a sensitivity analysis is conducted using the Latin hypercube Sampling (LHS) method to identify the most influential variables affecting the optimization objectives: heating energy use, cooling energy use, and thermal comfort (quantified by discomfort hours *"DH"*). They found that low-emissivity glazing, high thermal capacity and insulation levels for the opaque elements, and no/smallest shading for south facing façade are beneficial in achieving optimal thermal comfort and heating energy performance. Bre et al. [26] carried out a multi-objective optimization to improve energy efficiency and thermal comfort in a single-family house in Argentina. They used a novel metamodel-based approach by dynamic coupling between NSGA-II and ANN metamodels, which were trained previously by the results of building performance simulations. In total, 12 discrete and categorial design variables, such as shading dimension, solar absorptance, window type, roof type, and external/internal wall type, are considered input factors. It was claimed that the presented method is able to reduce the number of simulations by up to 75% without affecting the accuracy of the results. In addition to the abovementioned studies, some other similar studies exist [27–33] that are analyzed in Table 1 based on four criteria (i.e., multi-objective, multizonal modeling, reference case study, and comprehensive or specific input factors). It is clear that, except [26] conducted for a case study in a hot and humid climate, other reviewed studies either do not have a comprehensive approach to selecting the input factors for the optimization (i.e., they focus on specific elements such as HVAC control parameters, solar design parameters, etc.) or fail to fulfill at least one of the specified criteria.

Numerous studies have examined the risk of overheating and indoor thermal comfort in different types of buildings during heatwaves, with some focusing on specific regions and employing different analysis methods. Ozarisoy [34] studied thermal comfort conditions in a prototype terraced building located in Watford, UK, from May to September 2018. It was found that indoor operative temperatures remain relatively high during the heatwaves, ranging from 26.5 $^{\circ}C$ to 32.5 $^{\circ}C$. The situation is worse in the bedrooms on the first floor, where indoor operative temperatures exceed EN 15251 Category II upper limit for 15% of the hours. Laouadi et el. [35] assessed overheating risk in a typical detached house (assuming old and current construction practice) located in Ontario, Canada, during the extreme heatwave from 5th to 11th July 2010. They applied the CIBSE TM52 [36], Passive House

Table 1
Summary of some studies that optimized thermal comfort in residential buildings.

Author(s)	Country	Case study	Optimization method	Features			
				Multi-objective	Multizonal modeling	Reference case study	Comprehensive (C) or Specific (S) input factors
Chegari et al. (2021) [24]	Morocco	Two-floor residential unit	ANN coupled to MOPSO, MOGA, and NSGA-II	✓	✓	✓	S (envelope thermo-physical parameters)
Vukadinović et al. (2021) [25]	Serbia	Detached passive house	NSGA-II	✓	✓	×	S (Passive solar design factors)
Ebrahimi-Moghadam et al. (2020) [45]	Iran	Residential tower	GA(1)	✓	✓	×	S (light shelves)
Bre et al. (2020) [26]	Argentina	Single-family house	ANN coupled to NSGA-II	✓	✓	✓	C
Gou et al. (2018) [27]	China	Apartment building	ANN coupled to NSGA-II	✓	✓	×	C
Li et al. (2017) [28]	China	Simple model & typical residential unit	Proposed method, GenOpt®, and ANN	✓	✓	×	C
Ascione et al. (2015) [29]	Turkey & Italy	Six-story residential building	MPC(2)	✓	✓	✓	S (HVAC system control parameters)
Yu et al. (2015) [31]	China	Three-story typical residential building	ANN coupled to NSGA-II	✓	×	✓	C

(1) **GA:** Genetic Algorithm,
(2) **MPC:** Model Predictive Control

Institute (PHI) [37], and heat stress (using transient Standard Effective Temperature "t-SET" index) methods to analyze overheating considering four different passive measures (combination of interior and exterior solar shadings with window opening). The results showed that naturally ventilated buildings cannot fully satisfy the overheating criteria during the heatwaves according to the abovementioned methods. It was also found that older and leakier houses are less prone to overheating than highly-insulated and airtight buildings. Zhou et al. [38] analyzed overheating risk in a room (dimensions: 5 m × 3 m × 2.5 m) of a residential unit located in Zurich, Switzerland, during the heatwave from 24th July to 9th August 2018. Four different orientations (north, south, east, and west) are assumed for the test room, and 26.5 $^{\circ}C$ is set as the overheating threshold. The results showed 51.3%, 44.3%, 51.3%, and 35.7% hours of exceedance during the heatwave for east, south, west, and north-facing orientations, respectively, where indoor operative temperature and relative humidity reach up to 27.8 $^{\circ}C$ and 60.9%, respectively. In addition to the abovementioned studies, some other similar studies exist [39–44] that are analyzed in Table 2. Among the reviewed studies, only [41] incorporates future heatwaves in the analysis; however, only comfort indices are used for overheating evaluations. Other studies neglect climate change scenarios and fail to picture future overheating incidents under more severe heatwaves.

1.3. Knowledge gap, aim, and research questions

Despite several studies on building optimization and thermal comfort analysis during heatwave events, there is relatively less research that couples both. Most studies perform optimization to find the best combinations of passive design strategies but do not proceed with the evaluation of optimal solutions under extreme events. In addition, most studies dealing with overheating risk during heatwave events are performed for passive houses or assume that the cooling system is running without any disruption in air-conditioned ones. The latter is not the case in reality due to probable failure in the cooling system. In addition, very limited studies incorporate climate change scenarios to forecast the impact of aggravating heatwaves on overheating risks in buildings. Therefore, as members of the International Energy Agency (IEA) EBC Annex 80 – "Resilient cooling of buildings" project, we carried out this research to address the abovementioned knowledge gap inspired by the frameworks and guidelines developed within the project [46–48]. This research aims to broaden the knowledge on overheating risk evaluations in high-performance residential buildings during critical conditions in the context of climate change. The research questions are:

- Q1: What will be the changes in outdoor weather conditions assuming a plausible scenario for climate change in Brussels?
- Q2: How to optimize the building for final HVAC energy use and thermal comfort using passive design strategies?
- Q3: How will optimal solutions perform in current and future heatwave scenarios coinciding with the outage of the cooling system?

1.4. Paper contribution

This study contributes to the new body of knowledge from an international perspective by performing multi-objective optimization and overheating analysis for a case study in a temperate oceanic climate (Cfb) according to the Köppen-Geiger-Peel climate classification. Such a climate is particularly dominant in Western Europe, in addition to some other major cities around the world, such as Vancouver, Auckland, Canberra, Nairobi, etc. The results and findings can be generalized to those cities with some provisions. It should be mentioned that the applicability range of the results and findings of the current study is limited to the temperate

Table 2
Summary of some studies that analyzed overheating in residential buildings during heatwaves using multiple indices.

Author(s)	Country	Case study	Indices	Features			
				Climate change	Short-term (S) or Long-term (L) heatwaves	Static (S) or Adaptive (A) comfort model	Heat stress (H) or Comfort (C) indices
Ozarisoy (2022) [34]	UK	Three-story terraced building	Indoor Operative Temperature (IOpT), Relative Humidity (RH), & Percentage of Exceedance Hours (% EH)	×	L	S & A	C
Laouadi et al. (2020) [35]	Canada	Typical detached home	Percentage of Exceedance Hours (% EH), Degree Hours (DH), Daily Weighted Exceedance (DWE), & transient Standard Effective Temperature (t-SET)	×	S	S & A	H & C
Zhou et al. (2020) [38]	Switzerland	A room in a residential building	Indoor Operative Temperature (IOpT), Relative Humidity (RH), Heat Index (HI) & Percentage of Exceedance Hours (%EH)	×	L	S	H & C
Kwok et al. (2017) [39]	Hong Kong	Four types of public rental housing	Air Temperature (AT), Standard Predicted Mean Vote (SPMV), Adjusted Predicted Mean Vote (APMV), & Percentage of Exceedance Hours (%EH)	×	L	S & A	C
Porritt et al. (2012) [40]	UK	A row of three terraced house	Indoor Operative Temperature (IOpT) & Degree Hours (DH)	×	L	S	C
Sakka et al. (2012) [42]	Greece	Apartments & detached houses	Air Temperature (AT) & Percentage of Exceedance Hours (%EH)	×	S & L	S	C
Porritt et al. (2011) [41]	UK	A row of three terraced house	Air Temperature (AT), Degree Hours (DH), & peak occupied operative temperature reduction	✓	S	S	C

oceanic climate; therefore, similar studies must be conducted to achieve valid and reliable results concerning other climates. In addition, this paper considers a wide range of passive design strategies as input factors for the optimization of a benchmark nearly Zero-Energy terraced building in Belgium. The findings are representative and can be extended to other buildings in the same typology to enhance energy efficiency and thermal comfort. Furthermore, this paper performs overheating analysis under current and future heatwaves and provides a clear picture of climate change impact assessment in buildings that are being built according to the current legislation in Belgium. Last but not least, this paper analyzes overheating during heatwaves coinciding with the cooling system outage shedding light on the importance of building thermal analysis under abnormal conditions.

2. Methodology

Fig. 1 shows the Study Conceptual Framework (SCF) adopted for the current study. The methodology consists of two main stages. In the first stage, a multi-objective optimization is performed to minimize the final HVAC energy use and thermal comfort, considering 13 passive design strategies. Three optimal solutions are then selected on the resulting Pareto front to proceed with the second stage. In the second stage, the simulations are performed for the selected optimal solutions during the short-term heatwave events assuming the outage of the cooling system.

DesignBuilder v7.0.0 software is used in both stages, which is a Graphical User Interface (GUI) for the EnergyPlus simulation engine. EnergyPlus, developed by the U.S. Department of Energy

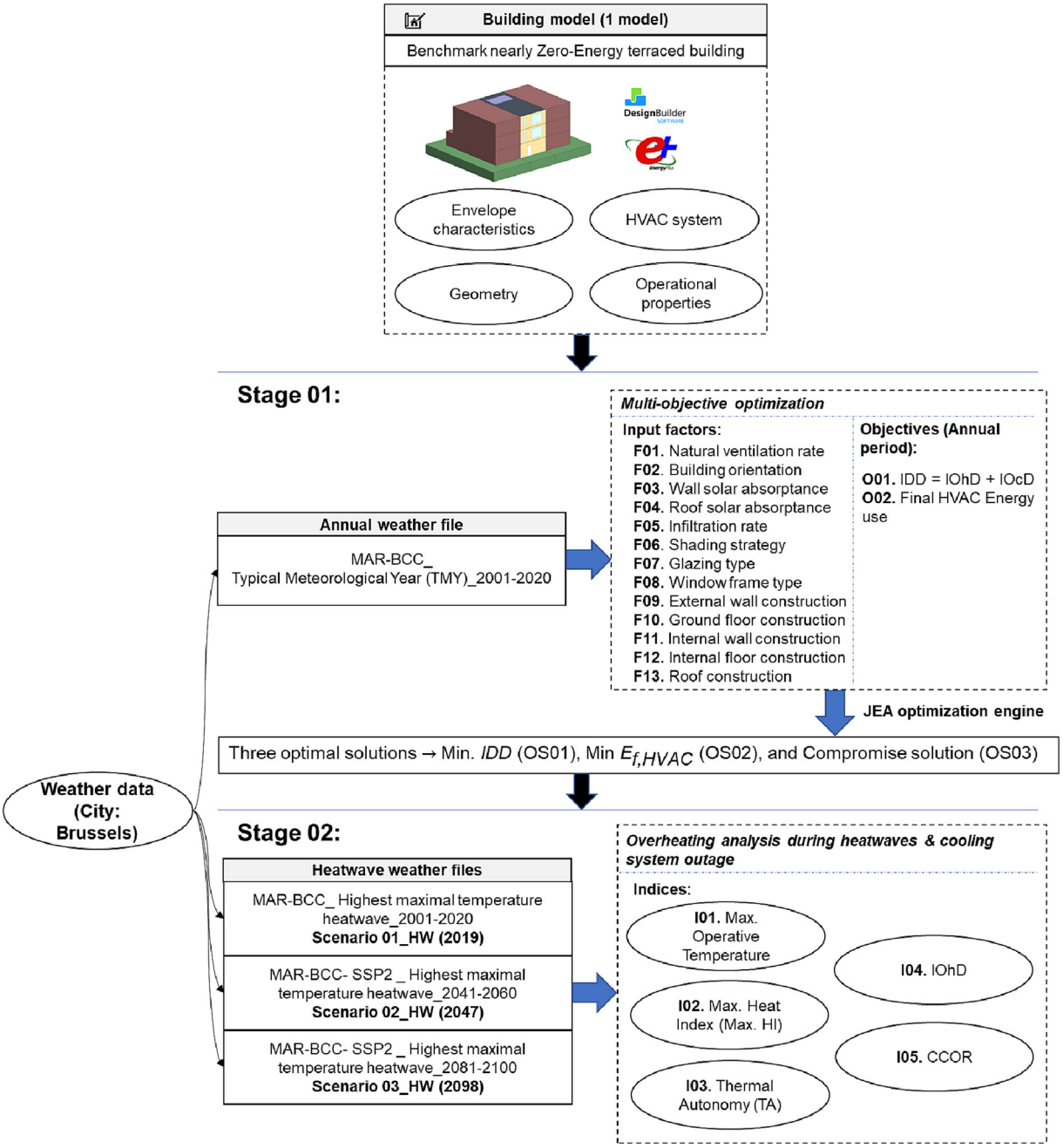

Fig. 1. Study Conceptual Framework (SCF).

(U.S. DOE), is accounted as one of the twenty major energy simulation programs [49], in which the simulation results are in close agreement with other well-known tools such as ESP-r, TRNSYS, DOE-2.1E, and IDA-ICE. DesignBuilder is validated based on a procedure specified by ANSI/ASHRAE 140, "*Method of Test for Evaluating Building Performance Simulation Software*" [50]. DesignBuilder uses Genetic Algorithm (GA) for optimization based on the Non-dominated Sorting Genetic Algorithm 2 (NSGA-II) method. NSGA-II method provides a feasible trade-off between a well-converged and well-distributed set of solutions and is highly effective in classifying the competing objectives. In this study, a combination of Energy Management System (EMS) and Python codes is also used to implement all the desired input variables for optimization. In total, over 4100 simulations are run in 48 h using a workstation with CPU: AMD 3990X – 64 × 2.9 GHz, Cache: 256 MB, RAM: 64 GB, and Graphics card: 24 GB (2 × 32 GB). The post-processing and visualizations are done using the CBE Clima tool [51] and a homemade MATLAB script [52].

2.1. Boundary conditions

This section is allocated to explain the boundary conditions of the current study. First, the focus is restricted to a case study located in a temperate oceanic climate (Cfb). Such a climate generally has cool summers and mild winters, with a relatively low-temperature gradient between different seasons. In Cfb climate regions, the Heating Degree Days (HDD) overlap the Cooling Degree Days (CDD); therefore, they are recognized as heating-dominated regions. In such regions, the building design concept is more on heat preservation during the cold seasons to reduce heating energy consumption. This results in highly insulated and airtight buildings that are more prone to overheating during the summer [53,54].

The second boundary condition assumed for this paper relies on the selection of single building typology representing the nearly Zero-Energy terraced dwellings in Belgium. This is because (i) newly built/renovated Passive house complying buildings are at a higher risk of overheating compared to less insulated old buildings [55–57], (ii) people spend most of their time at home [58], especially after the COVID pandemic and the rising tendency toward remote working [59], and (iii) overheating during the sleeping period at homes is identified as a critical risk for the occupants' health [60,61].

2.2. Building model

This paper selects a benchmark terraced dwelling in Belgium as the case study based on the work of [62]. The building is located in Woluwe-Saint-Lambert municipality in Brussels. As shown in Fig. 2, it was constructed in three floors and renovated in 2010 to comply with the nearly Zero-Energy Building (nZEB) requirements. The envelope was externally insulated during the renovation, and photovoltaic panels were added to the roof for on-site electricity generation of 3000 kWh/year. The multizonal building model includes the conditioned zones categorized as (i) living areas (living room and open kitchen as one zone), (ii) office room, (iii) bedrooms, and (iv) short-presence areas (two corridors, two bathrooms, one WC) [63].

Table 3 provides an overview of the general building's characteristics. The building has a total area of 259 m^2 and is occupied by a four-member family (two adults and two children). The occupancy schedules are derived differently for weekdays and weekends from ISO 18253–2 [33]. The lighting power density of 8 W/m^2 for the bedrooms and 10 W/m^2 for other zones are set based on the data collected from the surveys. The lighting densities are adjusted for the winter season and validated using the reports published by IP Belgium and the Flemish Energy Agency (FEA). The building model in this paper is obtained from [63], which has been checked against the public statistics and verified through model calibration and utility bill comparison between 2015 and 2019.

In its original mode, the building is naturally ventilated and heated by a gas-fired boiler coupled with water radiators. In addition, a mechanical ventilation system with heat recovery operates to provide a minimum fresh air of 25 m3/h during the occupied hours according to the Belgian norm NBN D50-001. Based on the findings of [64,65], this paper replaces the gas-fired boiler with a reversible air-to-water heat pump to provide heating and cooling along with natural ventilation (mixed-mode). The set-point temperatures for heating and cooling modes and the minimum and maximum indoor temperatures for natural ventilation are listed in Table 3. The HVAC components' design flow rates and thermal capacities are auto-sized by EnergyPlus based on the building configuration and external weather conditions using the ASHRAE siz-

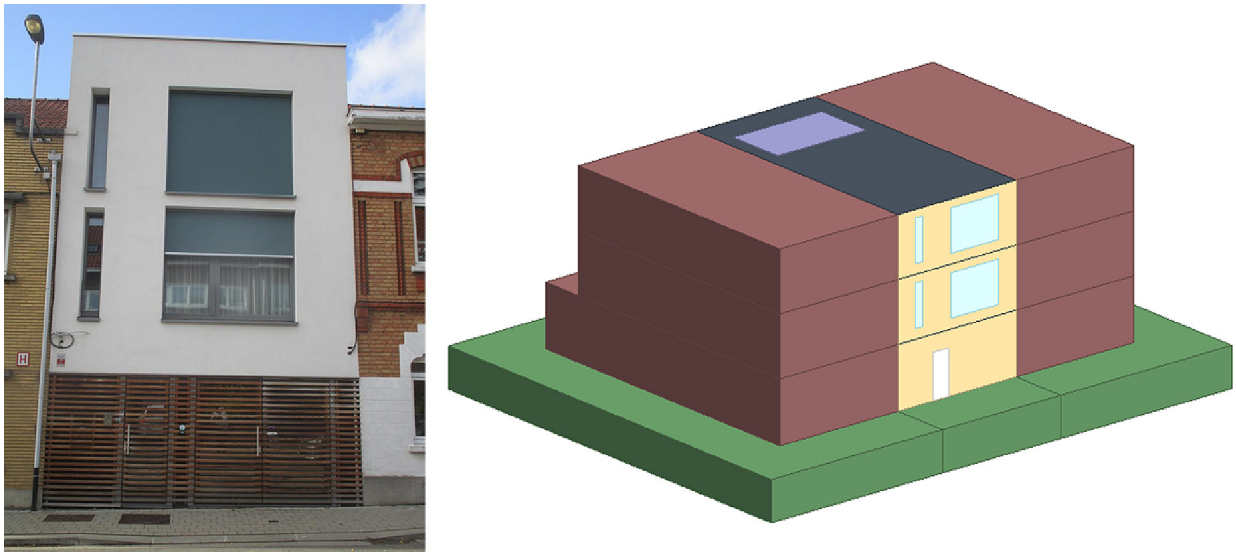

Fig. 2. The benchmark nearly Zero-Energy terraced dwelling in Belgium: (left) south-facing façade and (right) DesignBuilder simulation model.

Table 3
General description of the case study's construction, operational, and HVAC characteristics derived from [62,64].

Description	Value
Number of floors	3
Total area [m^2]	259
Conditioned area [m^2]	173
Unconditioned area [m^2]	86
Number of occupants	4
Total volume [m^3]	873
Window-wall ratio [%]	19
Occupancy density [m^2/person]	43
Occupancy, lighting, and equipment schedules	Ref. [62]
Lighting power density [W/m^2]	8 (bedrooms) & 10 (other zones)
Holidays	(Easter) start: 30/03 end: 05/04, total: 7 days (Summer) start: 01/08 end: 155/08, total: 15 days (All saint's day) start: 28/10 end: 05/11, total: 7 days (Christmas) start: 24/12 end: 01/01, total: 7 days
HVAC System type	Reversible air-to-water heat pump + mechanical ventilation
Heated and cooled zones	Heated: Living & kitchen, office, bedroom 01, bedroom 02, bedroom 03, corridors, WC, bathroom 01, and bathroom 02; Cooled: Living & kitchen, office, bedroom 01, bedroom 02, and bedroom 03
HVAC schedule	≡ occupancy schedules in Ref. [62]
Heating and cooling capacities [W]	Auto-sized to design days
Heating and cooling schedules [h]	Occupied hours
Set-point temperatures [°C]	21 °C for heating (living & kitchen, and office); 18 °C for heating (bedrooms and short-presence areas, e.g., corridors, bathrooms, and WC); 24 °C for cooling (all areas)
Maximum indoor temperature for natural ventilation [°C]	23.5 °C for all areas
Minimum indoor temperature for natural ventilation [°C]	21.5 °C for living & kitchen and office; 19 °C for bedrooms and short-presence areas, e.g., corridors, bathrooms, and WC
Minimum ventilation rate [m^3/h]	25

ing method [66]. The auto-sizing feature sizes the HVAC components in a way to fulfil the heating/cooling loads for all periods except for more extreme conditions than the design days (i.e., there is still a chance of overcooling/overheating in the building). In line with the authors' previous works [47,64], the availability schedule of the HVAC system is considered identical to the occupancy schedules defined in [62].

2.3. Climate data

Obtaining high-quality and detailed climate data is crucial in any study related to climate change and adaptation decisions [67]. The current study uses climate data based on the General Circulation Model (GCM) outputs. GCM outputs are not directly applicable to building simulations due to their high spatial and temporal resolution. They should be transformed using statistical or dynamical downscaling techniques in order to generate compatible weather data. For this aim, a dynamical downscaling technique called the Regional Climate Model (MAR) *"Modèle Atmosphérique Régional"* (in version 3.11.14) [68] was used to generate the weather data in this paper. MAR is calculated by coupling a three-dimensional atmospheric model to a one-dimensional transfer scheme between the surface, vegetation, and atmosphere [69]. MAR results in physically consistent climate parameters and extreme weather events and is widely adapted for Belgium [70,71].

Two different methods were used to ensure the validity of future weather data:

- **MAR ERA5:** In this method, MAR was initially forced every 6 h by its lateral boundaries (temperature, specific humidity, and etc.) based on the reanalysis ERA5 [72] assimilated by different sources of observation between 1980 and 2014. The sources of observation were in-situ weather stations, satellites, etc. Therefore, MAR ERA5 is assumed to be the reconstruction of the observed climate data.
- **MAR BCC-CSM2-MR:** In this method, MAR was forced based on the Earth System Model (ESM) BCC-CSM2-ME (mean temperature of all ESMs up to 2100 over Belgium) from the 6th Coupled Model Intercomparison Project (CMIP6). CMIP6 characterizes the average evolution of climate parameters between 1980 and 2014 based on observations and 2015–2100 based on Shared Socioeconomic Pathway (SSP) scenarios [73]. SSPs are used to project the Green House Gas (GHG) emission scenarios based on global socioeconomic evolution by 2100. In other words, they quantify the GHG emissions under different global climate policies. In total, there are five SSPs, i) SSP1-1.9 – CO_2 -emissions cut to net zero around 2050 (1.4 °C estimated global warming by 2100), ii) SSP1-2.6 – CO_2 emissions cut to net zero around 2075 (1.8 °C estimated global warming by 2100), iii) SSP2-4.5 – CO_2 emissions around current levels until 2050, then falling but not reaching net zero by 2100 (2.7 °C estimated global warming by 2100), iv) SSP3-7.0 – CO_2 emissions double by 2100 (3.6 °C estimated global warming by 2100), and v) SSP5-8.5 – CO_2 emissions triple by 2075 (4.4 °C estimated global warming by 2100) [74,75]. In this paper, the SSP2-4.5 scenario is selected, which is the most plausible scenario according to [76], in which the evaluation of 1184 IPCC AR5 [77] and 127 IPCC AR6 [1,74] scenarios are compared to observations over 2005–2020 [78] and projections to 2021–2050 from the International Energy Agency's (IEA) 2021 World Energy Outlook (WEO) [79]. From the perspective of the IPCC scenarios, it is evident from [76] that the globe is not now very far off the Fossil Fuel and Industry (FFI) emission trajectory envisioned in IPCC scenarios to be consistent with meeting 2 °C policy goals and all plausible scenarios fall between 2 °C and 3 °C by 2100 (global warming estimation in SSP2-4.5). This is also in line with the IPCC AR6 [1], which recently determined that mid-range scenarios (e.g., SSP2-4.5) are more likely and high-emission scenarios (e.g., SSP5-8.5) have a low likelihood.

MAR BCC-CSM2-MR was validated using the results of MAR ERA5 to confirm whether it can be used to calculate future climate data [68].

This paper uses the annual weather data for the optimization stage based on the protocol defined by ISO 15927–4 [80]. Accordingly, the Typical Meteorological Year (TMY) is used for the period 2001–2020 based on the outcomes of MAR BCC-CSM2-MR. TMYs are widely used by building designers and modelers [81] since they are accounted to be reasonably accurate and useful in estimating long-term building energy and thermal performance [82].

During the second stage of this paper, the heatwave weather data are used. According to the Royal Meteorological Institute (RMI) of Belgium, a heatwave is a period of a minimum of five consecutive days with a maximum air temperature higher than 25 $^{\circ}C$, in which at least three days have a maximum air temperature higher than 30 $^{\circ}C$ [83]. The above definition is static and does not consider the climate variations in different regions. In addition, a fixed threshold for heatwave definition leads to artifacts when comparing the data obtained from different ESMs, since each ESM has its own biases and variations. The heatwave weather data used in the second stage are derived based on a statistical method by [84] coupled to the RMI static heatwave definition. Therefore, they lack the abovementioned limitations. The calculation method was based on three principles, which can be found in [68]. All the heatwaves are characterized based on three criteria, including duration (number of consecutive days during the heatwave period), maximal temperature (maximum daily mean air temperature), and intensity (the cumulative difference between the air temperature and S_{deb} during the heatwave period, divided by the difference between S_{deb} and S_{pic}). S_{deb} and S_{pic} are 97.5%, and 99.5% percentiles of the reference period air temperature dataset, respectively. In this paper, the highest maximal temperature heatwaves are selected during three different periods, including 2001–2020 (historical scenario), 2041–2060 (mid-future scenario), and 2081–2100 (future scenario). The selection of the periods is based on the recommendations of the dynamic simulation guideline provided by the International Energy Agency (IEA) EBC Annex 80 – "Resilient cooling of buildings" project [46,85] and a previous study in the scientific literature [47]. All the weather data in this paper are obtained from [68].

2.4. Stages of analysis

As mentioned earlier, this paper consists of optimizing passive cooling design strategies (Stage 01) and a short-term analysis during heatwave events and the cooling system outage (Stage 02). The following sections (i.e., Section 2.4.1 and Section 2.4.2) are allocated to describe each stage and its corresponding indicators.

2.4.1. Stage 01: Optimization using passive design strategies

Optimization in building design is the practice of using mathematical models to formulate a design problem in order to select the optimal design solutions among many other alternatives. In this paper, the NSGA-II algorithm is used to determine non-dominated design solutions developed by the combinations of 13 passive design strategies (see Table 4) to minimize final HVAC energy use and Indoor Discomfort Degree (IDD). The NSGA-II multi-objective genetic algorithm method [86] is widely used to optimize the design of new buildings and the renovation of existing ones [87–89]. The NSGA-II is based on crowding distance sorting mechanisms and is defined by some main features such as generation population size, crossover probability, mutation probability, the maximum number of generations, and the number of objectives. Based on the literature analysis and considering the available computational capacity, the following parameters are set for the analysis in this paper, (i) generation population size = 50, (ii) crossover probability = 1, (iii) mutation probability = 0.4, (iv) the maximum number of generations = 400, and (v) number of objectives = 2.

In this paper, the input factors for optimization are selected among those representing passive and bioclimatic design strategies. For this aim, a set of 13 design strategies are chosen based on the literature review [90–93], in order to determine their relative impact on thermal comfort and energy performance of the studied model. Those strategies are applicable to the examined model considering its components and climate. All the input factors' characteristics, including type, minimum/maximum/step value (for numeric factors), and options (for non-numeric factors), are listed in Table 4. The objective functions are based on two indicators, final HVAC energy use ($E_{f,HVAC}$) for energy efficiency analysis and Indoor Discomfort Degree (IDD) for thermal comfort analysis. The final HVAC Energy use includes the electricity consumption of the compressor, condenser/evaporator pump, condenser/evaporator fan, and tank supplementary internal heating coil for the reversible air-to-water heat pump system. The optimization process is conducted using the Typical Metrological Year (TMY) weather data for the period 2001–2020 (see Section 2.3).

In this paper, the Indoor Discomfort Degree (IDD) indicator is proposed for thermal comfort assessment, inspired by the recommendations of the guidelines developed in the International Energy Agency (IEA) EBC Annex 80 – "Resilient cooling of buildings" project [46,48,94] and the scientific literature [47,64,95]. *IDD* [$^{\circ}C$] is a symmetric time-integrated thermal discomfort index that sums up Indoor Overheating Degree (IOhD) [$^{\circ}C$] and Indoor Overcooling Degree (IOcD) [$^{\circ}C$] [64,94]. *IOhD* and *IOcD* are multizonal indices that accumulate the heating and cooling degree hours over the total number of zonal occupied hours, respectively. The multizonal feature of *IOhD* and *IOcD* allows for the implementation of zone-specific thermal comfort models (i.e., static or adaptive) and requirements (e.g., comfort categories) tracking the zonal occupied hours. The formulas to calculate *IDD*, *IOhD*, and *IOcD* are as follows,

$$IDD = IOhD + IOcD \quad (1).$$

$$IOhD \equiv \frac{\sum_{z=1}^{Z}\sum_{i=1}^{N_{occ}(z)}\left[\left(T_{in,z,i}-T_{comf,upper,z,i}\right)^{+}\times h_{i,z}\right]}{\sum_{z=1}^{Z}\sum_{i=1}^{N_{occ}(z)} t_{i,z}} \quad (2).$$

$$IOcD \equiv \frac{\sum_{z=1}^{Z}\sum_{i=1}^{N_{occ}(z)}\left[\left(T_{comf,lower,z,i}-T_{in,z,i}\right)^{+}\times h_{i,z}\right]}{\sum_{z=1}^{Z}\sum_{i=1}^{N_{occ}(z)} h_{i,z}} \quad (3).$$

Where Z [-] is the total number of building zones, z is zone counter, $N_{occ}(z)$ [-] is the total number of occupied hours in zone z, i is hour counter, $T_{in,o,z}$ is the indoor operative temperature in zone z at hour i, $T_{comf,upper,z,i}$ is maximum comfort threshold in zone z at hour i, $T_{comf,lower,z,i}$ is the minimum comfort threshold in zone z at hour i. This paper refers to ISO 17772–1 standard to define the upper and lower limits of comfort (i.e., $T_{comf,upper,z,i}$ and $T_{comf,lower,z,i}$). ISO 17772–1 standard provides category-based static (Cat. I, Cat. II, Cat. II and Cat. IV) and adaptive (Cat. I, Cat. II, and Cat. III) thermal comfort criteria. This paper selects, (i) the static criterion that is recommended to actively heated and cooled buildings [47] and (ii) Category II that is recommended for new buildings and renovations [96]. As a result, $T_{comf,upper,z,i}$ and $T_{comf,lower,z,i}$ are set to 26 $^{\circ}C$ and 20 $^{\circ}C$, respectively, assuming a sedentary activity for the occupants (1.2 met) as well as clothing factors of 0.5 clo for summer and 1 clo for winter. It should be noted that the target zones for the calculation of *IDD* are living + kitchen, bedroom 01, bedroom 02, and office.

2.4.2. Stage 02: Overheating analysis during heatwaves and cooling system outage

In Stage 02, a set of optimal solutions obtained from Stage 01 is analyzed under short-term heatwave conditions coinciding with the outage of the cooling system. The heatwave weather data used

Table 4
The ranges/options of input factors for optimization.

	Factor	Type	Min. value Options	Max. value	Step	Number of values / options
F1	Natural ventilation rate [ac/h]	Discrete	1	5	2	3
F2	Building orientation [°]	Discrete	135	315	180	2
F3	Wall solar absorptance [-]	Discrete	0.40	0.90	0.10	6
F4	Roof solar absorptance [-]	Discrete	0.40	0.80	0.10	5
F5	Infiltration rate [ac/h]	Discrete	0.10	1.20	0.10	12
F6	Shading strategy(1)	Discrete	No shading, Electrochromic glazing, Roller blind, venetian blind			4
F7	Glazing type	Discrete	Thermochromic, U0.8(2)-SHGC0.2(3), U0.8-SHGC0.5, U0.8-SHGC0.8, U0.9-SHGC0.2, U0.9-SHGC0.5, U0.9-SHGC0.8, U1-SHGC0.2, U1-SHGC0.5, U1-SHGC0.8, U1.1-SHGC0.2, U1.1-SHGC0.5, U1.1-SHGC0.8, U1.2-SHGC0.2, U1.2-SHGC0.5, U1.2-SHGC0.8			16
F8	Window frame type	Discrete	Aluminum frame with no thermal break, Aluminum frame with thermal break, Painted wood, UPVC			4
F9	External wall construction	Discrete	U0.1-ThM1000(4), U0.1-ThM2000, U0.1-ThM3000, U0.2-ThM1000, U0.2-ThM2000, U0.2-ThM3000, U0.3-ThM1000, U0.3-ThM2000, U0.3-ThM3000			9
F10	Ground floor construction	Discrete	U0.1-ThM1000, U0.1-ThM2000, U0.1-ThM3000, U0.2-ThM1000, U0.2-ThM2000, U0.2-ThM3000, U0.3-ThM1000, U0.3-ThM2000, U0.3-ThM3000			9
F11	Internal wall construction	Discrete	U1-ThM1000, U1-ThM2000, U1-ThM3000, U1.5-ThM1000, U1.5-ThM2000, U1.5-ThM3000, U2-ThM1000, U2-ThM2000, U2-ThM3000			9
F12	Internal floor construction	Discrete	U0.8-ThM1000, U0.8-ThM2000, U0.8-ThM3000, U0.9-ThM1000, U0.9-ThM2000, U0.9-ThM3000, U1-ThM1000, U1-ThM2000, U1-ThM3000			9
F13	Roof construction	Discrete	U0.1-ThM1000, U0.1-ThM1000 + GR(5), U0.1-ThM2000, U0.1-ThM2000 + GR, U0.1-ThM3000, U0.1-ThM3000 + GR, U0.2-ThM1000, U0.2-ThM1000 + GR, U0.2-ThM2000, U0.2-ThM2000 + GR, U0.2-ThM3000, U0.2-ThM3000 + GR, U0.3-ThM1000, U0.3-ThM1000 + GR, U0.3-ThM2000, U0.3-ThM2000 + GR, U0.3-ThM3000, U0.3-ThM3000 + GR			18

(1) all shading devices are positioned outside and controlled by inside air temperature set-point of 24 °C during occupied hours
(2) U-Value (thermal conductivity) [W/m^{2}K],
(3) Solar Heat Gain Coefficient [-],
(4) Thermal Mass [KJ/m^{2}K], and
(5) Green Roof → substrate layer = 15 cm, drainage layer = 5 cm, plant height = 0.1 m, leaf reflectivity = 0.22, and leaf emissivity = 0.95 [97].

in this stage represents the heatwaves with the highest maximal temperature over three periods, including 2001–2020 (historical), 2041–2060 (mid-future), and 2081–2100 (future) (see Section 2.3).

Initially, a zonal thermal comfort analysis is carried out using three fit-to-purpose indices, including maximum operative temperature (derived from air temperature, mean radiant temperature, and air velocity), maximum Heat Index (HI) [98], and Thermal Autonomy (TA) [99]. *HI* metric, also known as the apparent temperature, is a metric that quantifies the human body's thermal sensation by coupling relative humidity (RH) and air temperature (T_{air}). *HI* [°C] metric is proposed by RELi 2.0. [98] guideline developed by U.S. Green Building Council (USGBC) to ensure thermal safety or thermally habitable conditions in buildings during the power outages. The formula to calculate *HI* has resulted from multiple regression analyses performed by [100] that requires adjustments for different ranges of air temperature and relative humidity. *HI* is calculated via Rothfusz's equation as below,

$$HI = -42.379 + 2.04901523 \times T_{air} + 10.1333127 \times RH - 0.22475541 \times T_{air} \times RH - 0.00683783 \times T_{air}^2 - 0.05481717 \times RH^2 + 0.00122874 \times T_{air}^2 \times RH + 0.00085282 \times T_{air} \times RH^2 - 0.00000199 \times T_{air}^2 \times RH^2 \quad (4).$$

$$where if RH < 13\% \& 26.66°C < T_{air} < 44.44°C : adjustment(subtracted) = [(13 - RH)/4] \times SQRT\{[17 - ABS(T - 95)]/17\}$$

$$if RH > 85\% \& 26.66°C < T_{air} < 30.55°C : adjustment(added) = [(RH - 85)/10] \times [(87 - T_{air})/5]$$

Where *SQRT* and *ABS* are square root function and absolute value, respectively. The US National Oceanic and Atmospheric Administration (NOAA) defines different ranges for *HI* index based on their effect on the human body (see Table 5). *HI* has become popular in environmental health research and has been widely used in previous studies [101–104].

Thermal Autonomy (TA) [%] index is defined as *"the percentage of the occupied time over a period where a thermal zone meets or*

Table 5
Classification of the Heat Index ranges based on the effect on the human body.

Classification	Heat Index	Effect on the body
Caution	26.6 °C – 32.2 °C	Possible fatigue with prolonged exposure and/or physical activity
Extreme caution	32.2 °C – 39.4 °C	Heat stroke, heat cramps, or heat exhaustion possible with prolonged exposure and/or physical activity
Danger	39.4 °C – 51.1 °C	Heat cramps or heat exhaustion likely, and heat stroke possible with prolonged exposure and/or physical activity
Extreme danger	More than 51.1 °C	Heat stroke highly likely

exceeds a given set of thermal comfort acceptability criteria through passive means only" [99]. *TA* puts forward the building construction as the main factor in defining the building's thermal performance. It is different from the conventional design approach of ensuring thermal comfort via a prosthetic mechanical system remedially. Therefore, *TA* fits to the aim of the current study at this stage while evaluating the building's thermal performance assuming the outage of the active cooling system. The formula to calculate *TA* is,

$$TA = \frac{\sum_{i=1}^{occupiedhours} wf_i}{\sum_{i=1}^{occupiedhours} h_i} where \begin{cases} wf_i = 1; T_{in} < T_{comfort,upper} \\ wf_i = 0; T_{in} > T_{comfort,upper} \end{cases} \quad (5)$$

Where wf_i is the weighting factor [-], T_{in} is indoor operative or air temperature [$^{\circ}C$], and $T_{comfort,upper}$ is the maximum temperature threshold.

Subsequently, the resistivity of building to overcome the increasing risk of overheating due to climate change is assessed using the Climate Change Overheating Resistivity (CCOR) index developed in [47]. *CCOR* metric shows the rate of change in indoor overheating risk represented by *IOhD* metric (See Section 2.4.1) with the change in outdoor weather conditions represented by the Ambient Warmness Degree (AWD) metric. In other words, it couples the indoor and outdoor environments to assess the ability of the building to withstand the warming outdoor weather conditions. *AWD* metric is used to quantify the severity of outdoor thermal conditions by averaging the Cooling Degree hours (CDh) calculated for a base temperature (T_b) of 18 $^{\circ}C$ over the total number of building occupied hours [94]. The formulas to calculate *AWD* and *CCOR* are,

$$AWD = \frac{\sum_{i=1}^{N_{occ,building}} [(T_{out,a,i} - T_b)^+ \times h]}{\sum_{i=1}^{N_{occ,building}} h_i} \quad (6)$$

$$\frac{1}{CCOR} = \frac{\sum_{Sc=1}^{Sc=M} (IOhD_{Sc} - \bar{IOhD}) \times (AWD_{Sc} - \bar{AWD})}{\sum_{Sc=1}^{Sc=M} (AWD_{Sc} - \bar{AWD})^2} \quad (7)$$

Where $T_{out,a,i}$ is the outdoor dry-bulb air temperature and *N* is the total number of building occupied hours, *Sc* is the weather scenario counter, *M* is the total number of weather scenarios, and $\bar{IOhD}$ and $\bar{AWD}$ are the averages of all *IOhDs* and *AWDs* calculated for different scenarios. Only the positive values of $(T_{out,a,i}\text{-}T_b)^+$ are taken into account in the summation. CCOR$>$ 1 means that the building is able to suppress the increasing outdoor thermal stress due to climate change, and CCOR$<$ 1 means that the building is unable to suppress the increasing outdoor thermal stress due to climate change. *CCOR* metric is recommended by Thermal Conditions Task Force [48] and Dynamic Simulation Task force [46] in (IEA) EBC Annex 80 – "Resilient cooling of buildings" project.

3. Results

3.1. Outdoor weather conditions

Fig. 3 shows the daily outdoor dry-bulb air temperature for the Typical Meteorological Year (TMY) generated for Brussels considering the 2001–2020 period based on the Regional Climate Model (MAR) "Modèle Atmosphérique Régional" (BCC-CSM2-MR). Heating Degree Days (HDD10 $^{\circ}C$) 929 $^{\circ}C$. days and Cooling Degree Days (CDD18 $^{\circ}C$) 294 $^{\circ}C$. days are calculated, showing that Brussels is generally a heating-dominated region with an annual average air temperature 10.83 $^{\circ}C$. January and February are the coldest months, with a mean air temperature 3.18 $^{\circ}C$ and 4.75 $^{\circ}C$, respectively. At the same time, July and August are the hottest months, with a mean air temperature 17.88 $^{\circ}C$ and 17.86 $^{\circ}C$, respectively. The minimum air temperature −11.5 $^{\circ}C$ (-7.1 $^{\circ}C$ assuming 1% percentile) is estimated during January, and the maximum air temperature 36.8 $^{\circ}C$ (29.8 $^{\circ}C$ assuming 99% percentile) is estimated during July. It is clear from Fig. 3 that the fluctuations between the day and night temperatures during the summer are higher than in the winter. In the cold months (January, February, and December), the average day and night temperature difference is 3 $^{\circ}C$; in the hot months (June, July, August, and September), it becomes 8 $^{\circ}C$. Also, April has the highest standard deviation 8.07 $^{\circ}C$, making it the month with the highest temperature gradient.

As explained in Section 2.3, the highest maximal temperature heatwaves are selected during three periods, including 2001–2020 (historical scenario), 2041–2060 (mid-future scenario), and 2081–2100 (future scenario). It should be noted that the mid-future and future scenarios are based on the SSP2-4.5 emission scenario. According to the heatwave characterization in [68], the highest maximal temperature heatwave occurred in 2019 during the 2001–2020 period and will occur in 2047 and 2098 during the 2041–2060 and 2081–2100 periods, respectively.

Fig. 4 shows the heat maps representing the distribution of outdoor air temperature for the years with the highest maximal temperature heatwave (i.e., 2019, 2047, and 2098). It also provides weather summaries, including Heating Degree Days (HDD10 $^{\circ}C$), Cooling Degree Days (CDD18 $^{\circ}C$), average, hottest, and coldest yearly air temperature, and annual cumulative horizontal solar radiation. According to the results, the average annual air temperature will increase 1.4 $^{\circ}C$ in 2047 and 4 $^{\circ}C$ in 2098 compared to 2019. *HDD10* $^{\circ}C$ decreases 18.29% in 2047 and 55.52% in 2098, whereas *CDD18* $^{\circ}C$ increases 39% in 2047 and 148.94% in 2098

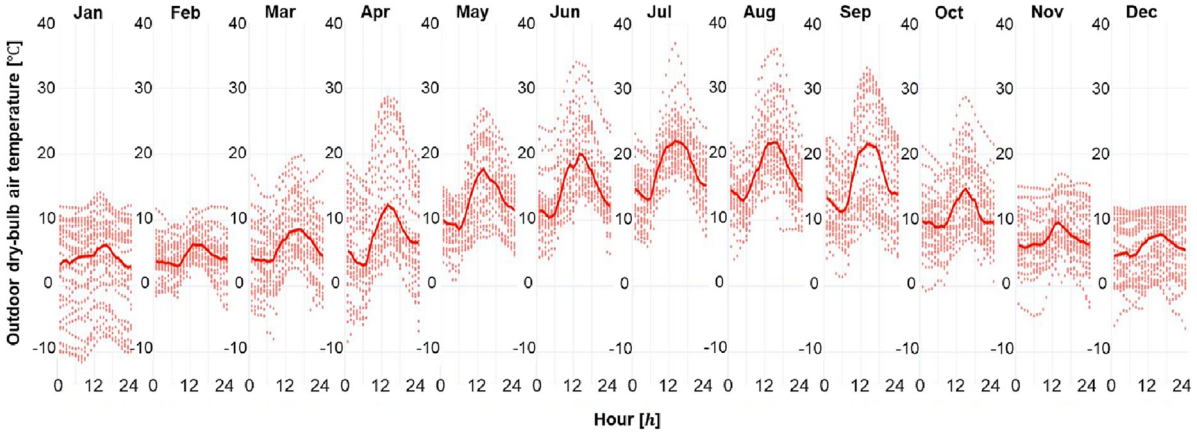

Fig. 3. The graph shows the daily outdoor dry-bulb temperature for different months in Brussels for the TMY of the period 2001–2020.

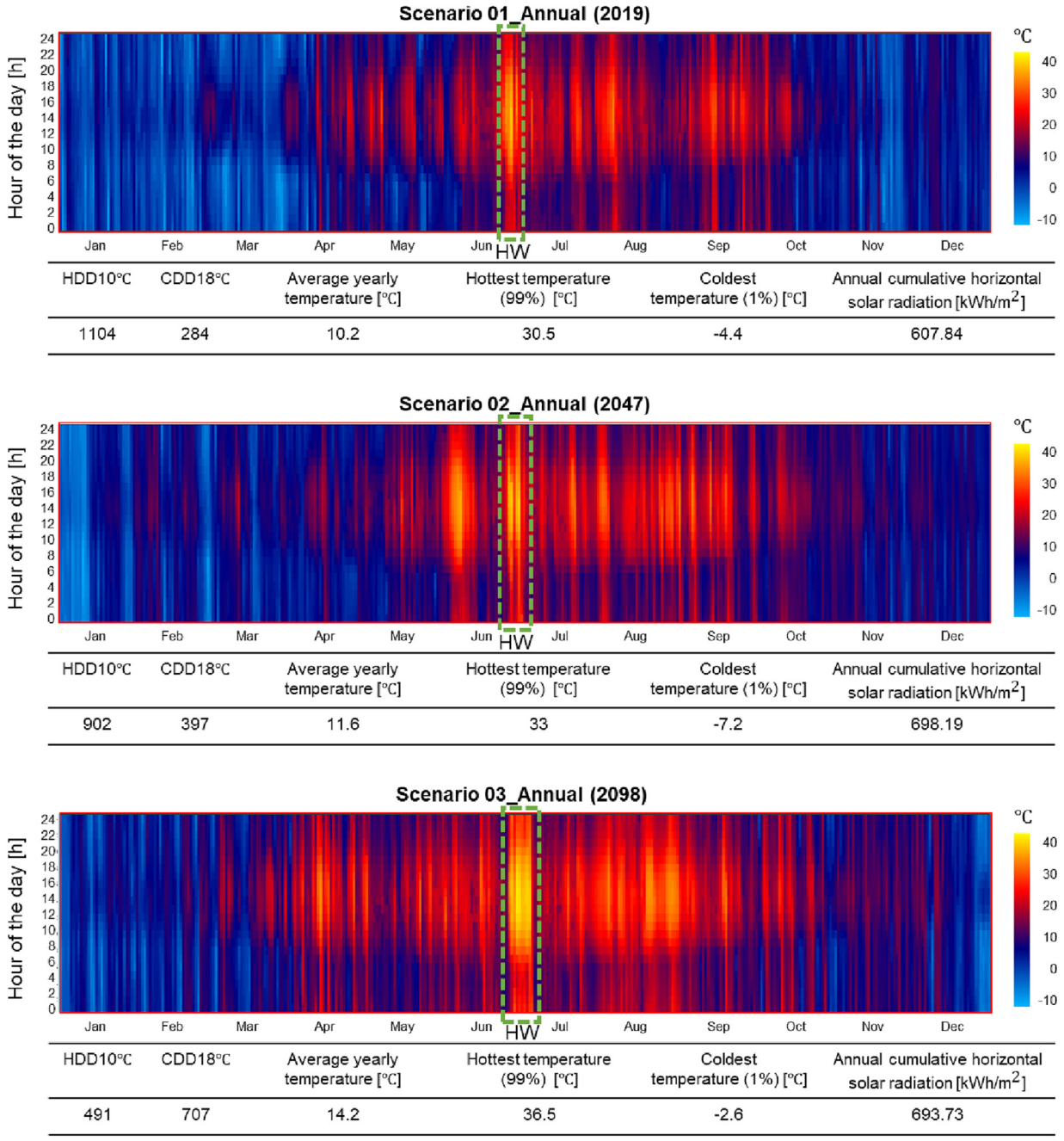

Fig. 4. The heat maps and weather summary for 2019, 2047 (under SP2-4.5 emission scenario), and 2083 (under SP2-4.5 emission scenario). The heatwaves are distinguished with green dashed lines. (For interpretation of the references to colour in this figure legend, the reader is referred to the web version of this article.)

compared to 2019. With the decrease of *HDD10* °*C* and the increase of *CDD18* °*C*, the average heating and cooling loads in buildings are expected to decrease and increase, respectively [105–107]. The highest hottest air temperature 36.5 °*C* is estimated in 2098, and the lowest coldest temperature −7.2 °*C* is estimated in 2047. Based on the climate data in this paper, the annual cumulative horizontal solar radiation inconsistently varies between 607.84 kWh/m^2 and 698.19 kWh/m^2 among the weather scenarios.

Fig. 5 depicts hourly outdoor dry-bulb air temperature during the highest maximal temperature heatwaves, and Table 6 summarizes their main characteristics. The heatwave detection is based on a statistical method [84] by calculating the three percentiles of the daily mean air temperature over the 2001–2020 period, including S_{int} = 23.8 °*C* (95th percentile) S_{deb} = 26.9 °*C* (97.5th percentile) and S_{pic} = 33.2 °*C* (99.5th percentile). The highest maximal temperature heatwaves generally start in late June and end by the end of the month or early July, depending on the duration of the event. According to the heatwave data used in this paper, the duration and average air temperature of heatwaves will increase with the continuation of global warming. The highest maximal temperature heatwave detected in 2019 lasted for 120 h (five days), while it increases to 168 h (seven days) by 2047 and 240 h (10 days) by 2098. Similarly, the average air temperature during the detected heatwaves in 2047 and 2098 will increase 3.28% and 12.15%, respectively, compared to the one in 2019. The intensity of heatwave as the cumulative difference between the air temperature and S_{deb}, divided by the difference between S_{deb} and S_{pic}, increases 115% by 2047 and 498% by 2098 due to the increase in temperature and duration of future heatwaves.

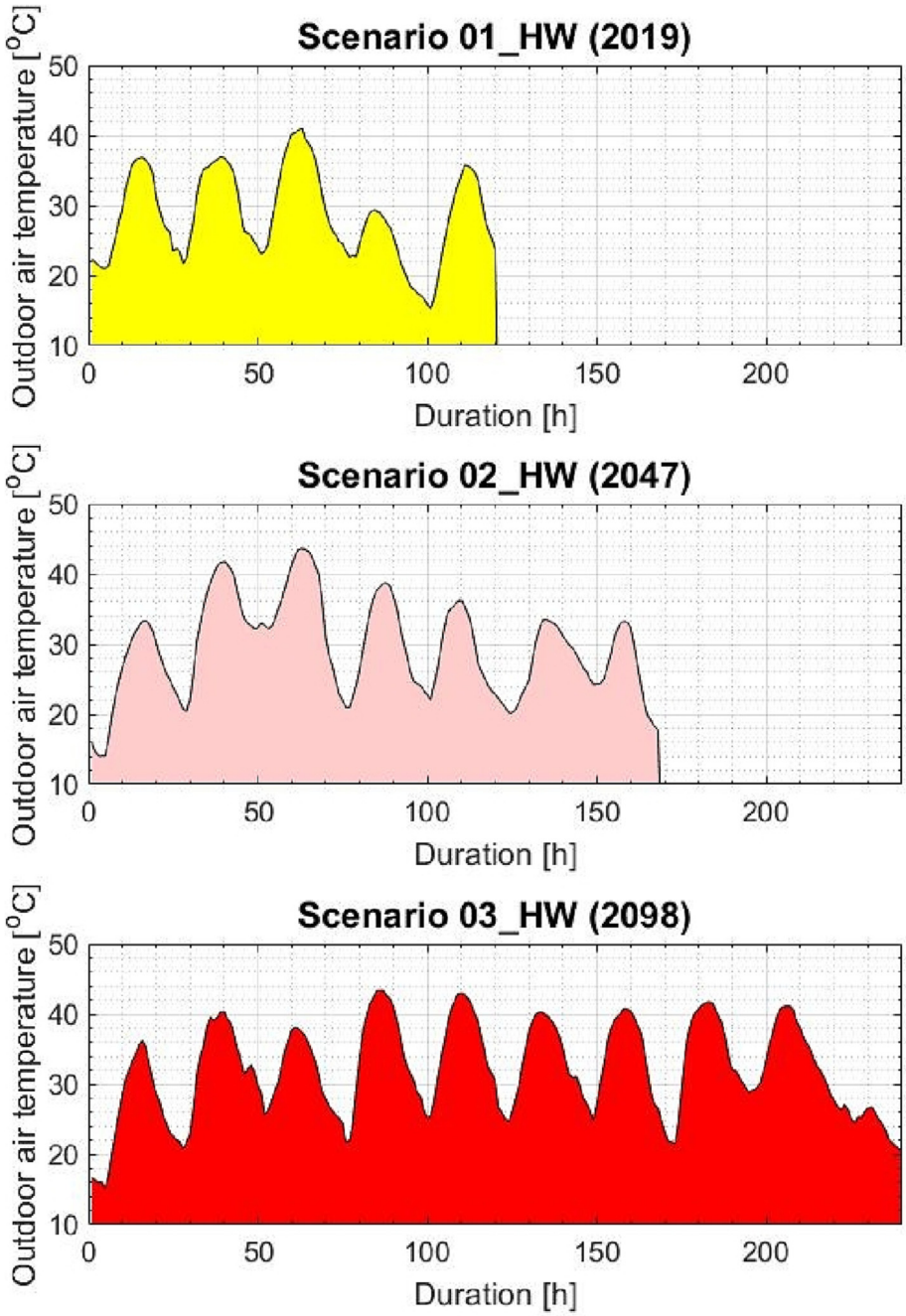

Fig. 5. Hourly outdoor air temperature during the highest maximal temperature heatwaves detected in 2019 for 2001–2020, 2047 for 2041–2060, and 2098 for 2081–2100.

Table 6
Summary of main parameters characterizing the three highest maximal temperature heatwaves: Scenario 01 HW (2019), Scenario 02 HW (2047), and Scenario 03 HW (2098).

	Scenario 01_HW (2019)	Scenario 02_HW (2047)	Scenario 03_HW (2098)
Date	25 Jun-29 Jun	25 Jun-01 Jul	26 Jun-05 Jul
Duration [days]	5	7	10
Intensity [-]	1.38	2.98	8.29
Max. Air Temperature [°C]	41.02	43.64	43.37
Avg. Air Temperature [°C]	28.64	29.58	32.12

3.2. Optimal solutions

Fig. 6 shows the optimization solution space to minimize final HVAC energy use ($E_{f,HVAC}$) and Indoor Discomfort Degree (IDD). The optimization problem can be mathematically expressed as,

$$min\{E_{f,HVAC}(x), IDD(x)\} for x \in X subject to WD(x) = TMY_{2001-2020} (8)$$

In multi-objective optimization, a set of solutions that are non-dominated by each other but are superior to the rest of solutions in the search space are denoted as the Pareto front or set of the optimal solutions in the space of objective functions. This means that

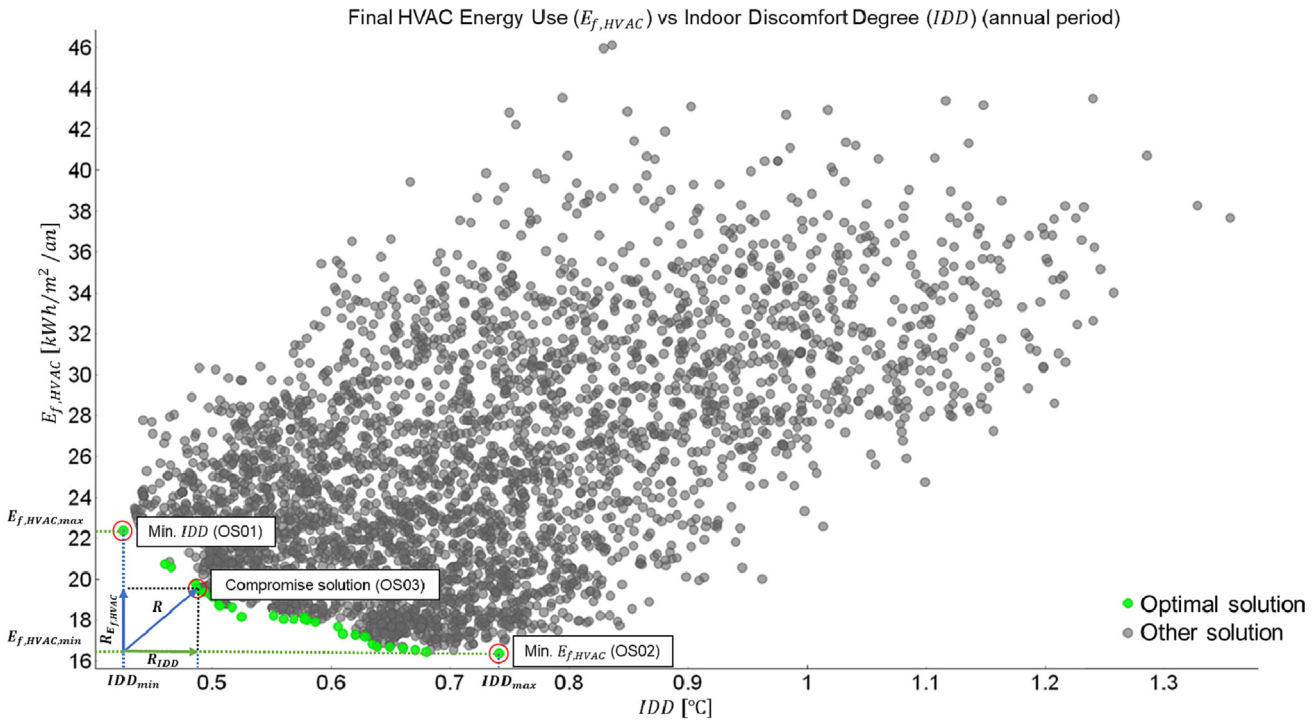

Fig. 6. Scatter plot of final HVAC energy use ($E_{f,HVAC}$) vs. Indoor Discomfort Degree (IDD) for all optimization cases, with green Pareto front and three optimal solutions distinguished. (For interpretation of the references to colour in this figure legend, the reader is referred to the web version of this article.)

no single solution can be found that is superior to all other solutions in terms of all objectives, making it impossible to simultaneously improve all objectives by altering the vector of design variables in a Pareto front made up of numerous non-dominated solutions. As a result, each solution of the Pareto front includes at least one objective inferior to another solution in that Pareto front, although both are superior to others in the rest of search space. In this paper, the selection of optimal solutions from the resulting Pareto front depends on the trade-off between both objective functions. As illustrated in Fig. 6, the Pareto front can be normalized considering the minimum and maximum values of the objective functions via coefficients $R_{E_{f,HVAC}}$ and R_{IDD}. The optimal solution OS01 is the most thermally comfortable solution (i.e., $R_{IDD} = 0$) with the highest final HVAC energy use (i.e., $R_{E_{f,HVAC}} = 1$). Differently, the optimal solution OS02 is the most energy-efficient solution (i.e., $R_{E_{f,HVAC}} = 0$) with the highest discomfort (i.e., $R_{IDD} = 1$). In addition, the optimal solution OS03 (or compromise solution) is selected as a trade-off, using $R_{E_{f,HVAC}}$ and R_{IDD} weighting factors (Eq. (9) and Eq. (10)). The compromise solution OS03 is characterized by the minimum value of $\bar{R}$ using the following equations,

$$f(\vec{x})_{OS03} = R_{E_{f,HVAC}}.E_{f,HVAC}(\vec{x}_{E_{f,HVAC},R_{E_{f,HVAC}}}) + R_{IDD}.IDD(\vec{x}_{IDD,R_{IDD}}) \quad (8)$$

$$R_{E_{f,HVAC}} = \frac{E_{f,HVAC}(\vec{x}_{E_{f,HVAC},R_{E_{f,HVAC}}}) - E_{f,HVAC_{min}}}{E_{f,HVAC_{max}} - E_{f,HVAC_{min}}} \quad (9)$$

$$R_{IDD} = \frac{R_{IDD}.IDD(\vec{x}_{IDD,R_{IDD}}) - IDD_{min}}{IDD_{max} - IDD_{min}} \quad (10)$$

$$\bar{R} = \sqrt{R^2_{E_{f,HVAC}} + R^2_{IDD}} \quad (11)$$

Table 7 summarizes the combinations of input factors and the outputs for the three selected optimal solutions (OS01, OS02, and OS03). F1-F13 are the input factors considered during the optimization process (see Table 4) that characterize each optimal solution. In addition to the optimization objectives/outputs, Table 7 lists additional outputs such as cooling energy use, heating energy use, Indoor Overheating Degree (IOhD), and Indoor Overcooling Degree (IOcD). In order to get the parameter values in Table 7, the optimization output (with a distinction of Pareto front and other solutions) is exported in.csv format from DesignBuilder, which includes all characteristics (i.e., input factors and outputs) of each solution. The exported.csv file is then imported into the Orange data analysis and visualization tool. Using the interactive feature in Orange, initially, the input factors' and outputs' values for the Min. *IDD* (OS01) and Min $E_{f,HVAC}$ (OS02) cases are extracted and recorded. Subsequently, the $\bar{R}$ is calculated for the rest of the solutions in the Pareto front to find the case with minimum $\bar{R}$ value (i.e., compromise solution) and extract corresponding input factors' and outputs' values.

It should be noted that $E_{f,HVAC}$ and *IDD* for the base case are 24.19 kWh/m^2 and 0.80 °*C*, respectively. OS01 has the lowest *IDD* value of 0.425 °*C* and the highest $E_{f,HVAC}$ value of 22.37 kWh/m^2 among all optimal solutions. On the other hand, OS02 has the highest *IDD* value of 0.741 °*C* and the lowest $E_{f,HVAC}$ value of 16.36 kWh/m^2 among all optimal solutions. OS03 has *IDD* value of 0.487 °*C* and $E_{f,HVAC}$ value of 19.53 kWh/m^2, falling between the minimum and maximum ranges of IDD and $E_{f,HVAC}$ owned by OS01 and OS02. OS01 has 2118.31 kWh higher cooling energy use, 674.4 kWh lower heating energy use, 91% higher overheating discomfort, and 44% lower overcooling discomfort compared to OS02. It is since: (i) the south-oriented zones that are more exposed to the sun in S01 (i.e., living + kitchen and bedroom 02 zones) have larger glazing areas than S02 (i.e., bedroom 01 and office zones), (ii) south-oriented zones (with larger glazing areas) in S01 has relatively higher occupancy hours compared to S02 (note that the HVAC operates and *IDD* is calculated during occupied hours; e.g., the living + kitchen zone with higher occupancy hours has more influence on the final HVAC energy use and *IDD* than the office), (iii) the solar heat gains through the envelope and glazing areas is higher in S01 than S02 due to higher wall solar absorptance, roof solar absorptance, and Solar Heat Gain Coefficients (SHGC) of windows.

Table 7
The characteristics of the selected optimal solutions: minimum Indoor Discomfort Degree (IDD) case (OS01), minimum final HVAC energy use ($E_{f,HVAC}$) case (OS02), and compromise solution case (OS03).

Optimal solutions													
Min. IDD (OS01)	**Factors**												
	F1	F2	F3	F4	F5	F6	F7	F8	F9	F10	F11	F12	F13
	5	135	0.50	0.60	0.10	Roller blind	U0.8-SHGC0.8	UPVC	U0.1-ThM3000	U0.1-ThM2000	U1-ThM3000W	U1-ThM3000W	U0.1-ThM3000 + GR
	Outputs												
	Final HVAC energy use [kWh/m^2]	Cooling energy use [kWh]	Heating energy use [kWh]	IDD [°C]	IOcD [°C]	IOhD [°C]							
	22.37	2435.01	1331.18	0.425	0.413	0.012							
Min. $E_{f,HVAC}$ (OS02)	**Factors**												
	F1	F2	F3	F4	F5	F6	F7	F8	F9	F10	F11	F12	F13
	5	315	0.40	0.40	0.10	Roller blind	U0.8-SHGC0.2	UPVC	U0.1-ThM3000	U0.1-ThM1000	U1-ThM3000W	U0.8-ThM3000	U0.1-ThM2000 + GR
	Outputs												
	Final HVAC energy use [kWh/m^2]	Cooling energy use [kWh]	Heating energy use [kWh]	IDD [°C]	IOcD [°C]	IOhD [°C]							
	16.36	316.70	2005.58	0.741	0.741	0.001							
Compromise solution (OS03)	**Factors**												
	F1	F2	F3	F4	F5	F6	F7	F8	F9	F10	F11	F12	F13
	5	135	0.80	0.50	0.10	Roller blind	U0.8-SHGC0.5	Painted wood	U0.1-ThM3000	U0.1-ThM1000	U1-ThM3000W	U1 - ThM3000	U0.1-ThM3000 + GR
	Outputs												
	Final HVAC energy use [kWh/m^2]	Cooling energy use [kWh]	Heating energy use [kWh]	IDD [°C]	IOcD [°C]	IOhD [°C]							
	19.53	1535.56	1559.79	0.487	0.487	0.004							

There are some factors that are common between the selected optimal solutions. The first common factor is the natural ventilation rate of 5 ac/h, which is the maximum specified value. This is in line with the findings of previous research [94,108–110] on the positive impact of high natural ventilation rates on improved cooling energy efficiency and summer comfort. It is since high rates of natural ventilation in mixed-mode buildings can adequately provide fresh outdoor airflow to maintain comfort during intermediate and summer seasons and delay the operation of active cooling systems. However, its potential is expected to diminish with the continuation of global warming [94,108,110,111]. The second common factor is the infiltration rate of 0.1 ac/h, which is the minimum specified value. Previous research [112–114] also confirmed that the infiltration rate negatively correlates with HVAC energy consumption and thermal comfort in buildings. It is because the infiltration rate is an uncontrolled phenomenon and consistently blows cold air in the winter and hot air in the summer into the building, adding to the heating and cooling loads. The third common factor is the lowest specified U-value for building envelope components. This shows that high insulation levels in an actively heated and cooled building in a temperate climate contribute to both energy-saving and thermal comfort. It is because high insulation levels can prevent the unwanted heat flux from the indoor environment in the winter and to the indoor environment in the summer. The same result is achieved in [115] for an envelope-dominated building with low levels of internal gains in a temperate climate. The fourth common factor is the highest specified thermal mass value of 3000 KJ/m^{2}K for envelope components. High thermal mass sets a high heat storage capacity for the building. It can help dampen the hot and cold peak temperatures, and if coupled with active systems, it helps in lowering the overall HVAC energy consumption [116]. The fifth common factor is the integration of green roofs. Like insulation, green roofs enhance the roofs' insulation, minimizing heat transfer [117]. Therefore, they can help reduce heating and cooling loads and improve thermal comfort in air-conditioned buildings [118]. The sixth common factor is the application of roller blinds as a shading strategy. Even though operable shading devices have limited benefits in lowering heating loads and overcooling discomfort, they are helpful in reducing cooling loads and overheating discomfort. According to the optimization objectives in this study, roller blinds are the best choice for achieving optimal thermal comfort and final HVAC energy use.

3.3. Thermal comfort assessment during heatwaves for optimized solutions

3.3.1. Zonal analysis

Fig. 7, Fig. 8, and Fig. 9 show the zonal indoor operative temperature for OS01, OS02, and OS03 during Scenario 01 HW (2019), Scenario 02 HW (2047), and Scenario 03 HW (2098) concurrent with the outage of the cooling system. Full-year simulations are per-

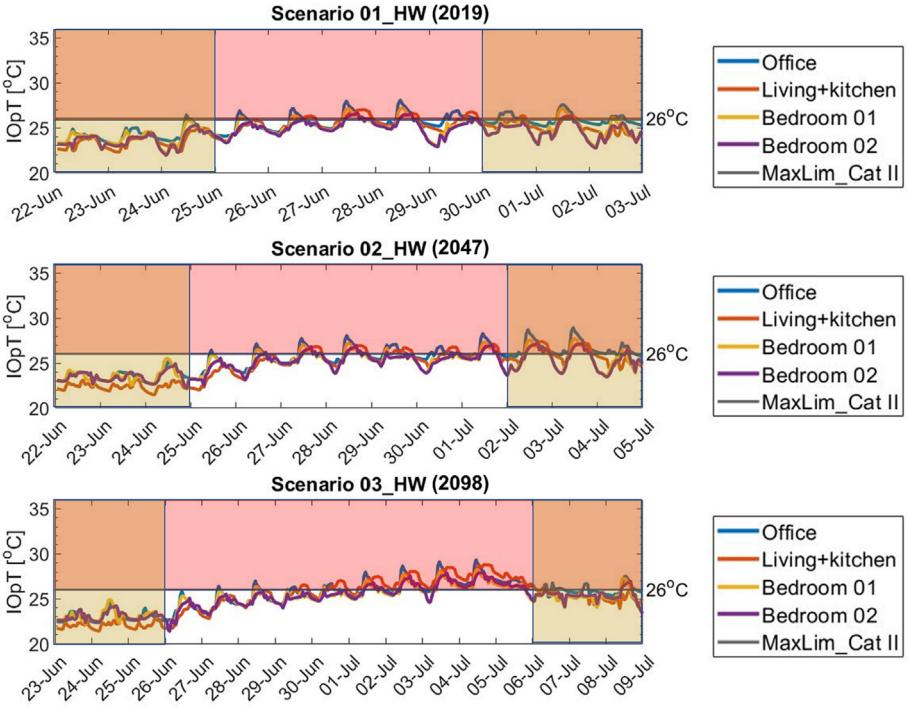

Fig. 7. The plots show the indoor operative temperature for different zones during the three heatwave scenarios for OS01 (including three days shoulder periods).

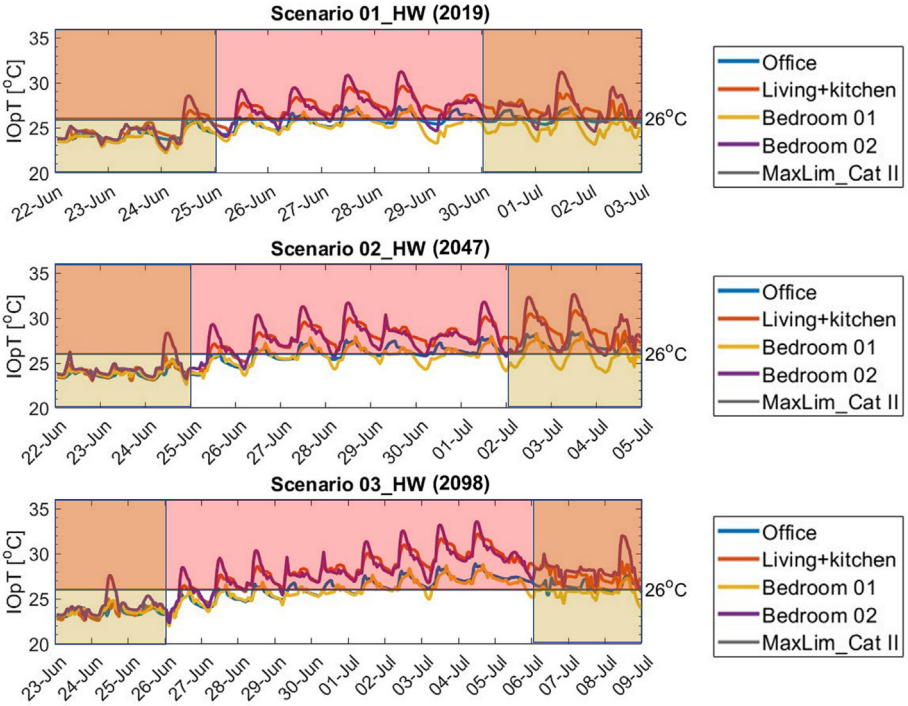

Fig. 8. The plots show the indoor operative temperature for different zones during the three heatwave scenarios for OS02 (including three days shoulder periods).

formed; only heatwaves and three-days shoulder periods are reported in the graphs. The shoulder periods are intended to indicate the building's thermal state before and after the heatwave occurrence.

The results show that OS02 is the only case that can fully maintain the indoor operative temperature within the comfort limits before the heatwaves start by only relying on passive measures. It means that OS01 and OS02 require active cooling to prevent overheating even during normal conditions. During the heatwaves, all three optimal solutions deviate from the maximum comfort limit of 26 $^{\circ}C$ (according to the Cat II static comfort model in ISO 17772–1) by different extents. For OS01, the maximum operative temperature reaches 32.86 $^{\circ}C$ in the most critical zone (i.e., bedroom 02) in the 2019 heatwave and increases up to 34.53 $^{\circ}C$ in the 2098 heatwave. For OS02, the maximum operative temperature reaches 28.09 $^{\circ}C$ in the most critical zone (i.e., office) in the

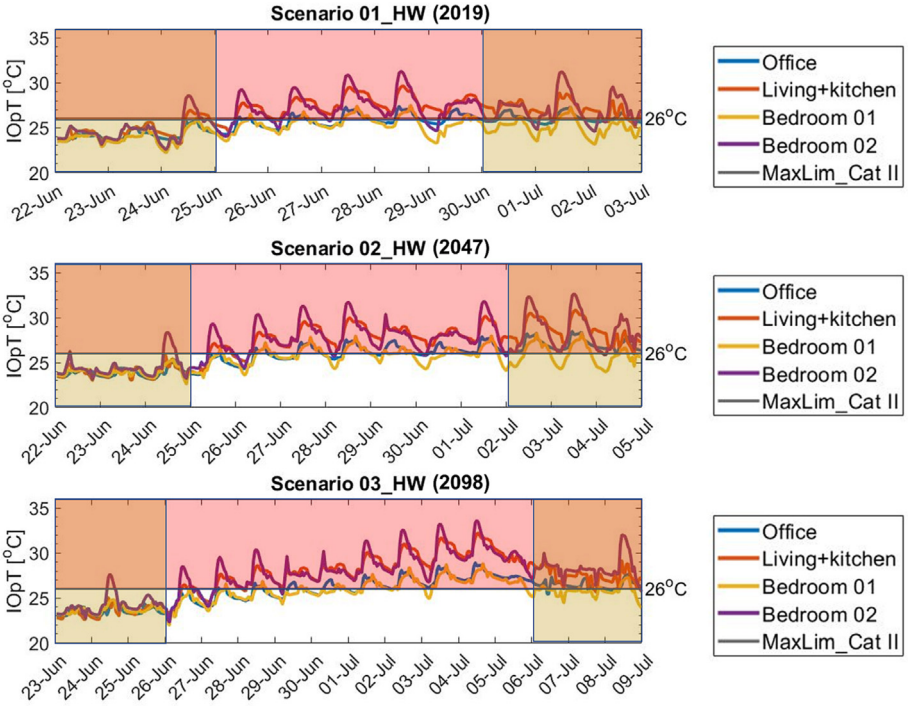

Fig. 9. The plots show the indoor operative temperature for different zones during the three heatwave scenarios for OS03 (including three days shoulder periods).

2019 heatwave and increases up to 29.35 °*C* in the 2098 heatwave. For OS03, the maximum operative temperature reaches 31.27 °*C* in the most critical zone (i.e., bedroom 02) in the 2019 heatwave and increases up to 33.64 °*C* in the 2098 heatwave. Furthermore, the indoor operative temperatures for the bedrooms significantly exceed, in all cases, the healthy sleeping temperature limit of 24 °*C* recommended by the World Health Organization (WHO). The results also show that non of the cases are able to recover right away after the termination of the heatwave period. The situation is worse for OS01 and OS03, in which the indoor operative temperatures remain at similar ranges as during the heatwaves.

Table 8 summarizes the zonal maximum operative temperature, maximum Heat Index (HI), and Thermal Autonomy (TA) for OS01, OS02, and OS03 during Scenario 01 HW (2019), Scenario 02 HW (2047), and Scenario 03 HW (2098) concurrent with the outage of the cooling system. According to RELi 2.0, *HI* should not go beyond 32.2 °*C*, corresponding to the "Extreme Caution" threshold (see Table 5) for residential units during the hot season. The results show that OS01 and OS02 fail to keep the abovementioned limit for Bedroom 02 in all three heatwave scenarios. The maximum *HI* values between 33.61 °*C* and 34.43 °*C* result for bedroom 02 in OS01 and between 32.29 °*C* and 32.80 °*C* in OS02. Therefore, there is a risk of heat stroke, cramp, or exhaustion for the occupants in Bedroom 02 with prolonged exposure and/or physical activity. On the other hand, OS02 can successfully maintain the maximum threshold of 32.2 °*C* in all scenarios.

Thermal Autonomy (TA) index correlates thermal comfort, building fabric, building operation, and climate [99]. It shows to what extent the building is able to maintain the comfort criteria autonomously (i.e., without the need for active heating and cooling) during occupied hours. In general, climate change causes a decrease in *TA* during heatwaves between 17% and 28% in selected optimal solutions. OS01 has *TA* values of 37.30% in Scenario 01_HW (2019), 32.68% in Scenario 02_HW (2047), and 28.056% in Scenario 03_HW (2098) averaged over all zones. OS02 has *TA* values of 83.70% in Scenario 01_HW (2019), 73.23% in Scenario 02_HW (2047), and 69.14% in Scenario 03_HW (2098) averaged over all zones. OS03 has *TA* values of 57.1% in Scenario 01_HW (2019), 43.17% in Scenario 02_HW (2047), and 40.68% in Scenario 03_HW (2098) averaged over all zones. Consequently, OS02 and OS01 are identified as the most autonomous and the least autonomous cases during the heatwaves, respectively.

3.3.2. Resistivity to overheating impact of climate change

The analyses of the Indoor Overheating Degree (IOhD), Ambient Warmness Degree (AWD) and Climate Change Overheating Resistivity (CCOR) are presented in this section. *IOhD* represents the frequency and intensity of overheating by implementing zonal comfort criteria. *AWD* shows the outdoor thermal severity by accumulating the cooling degree hours averaged over total building occupied hours. *CCOR* couples *IOhD* and *AWD* (i.e., couples indoor and outdoor environments) to quantify the extent of variation in *IOhD* corresponding to a variation in *AWD*. In other words, *CCOR* is the inverse of the slope of the linear regression line between *IOhD* and *AWD*. As shown in Fig. 10, there is a direct correlation between IOhD and AWD; that is, when *AWD* increases, *IOhD* increases as well. The severity of heatwaves is represented by *AWD* in Fig. 10 as follows: AWD for the 2019 heatwave = 4.871 °*C*, AWD for the 2047 heatwave = 6.3 °*C*, and AWD for the 2098 heatwave = 8.855 °*C*.

This study calculated the highest *IOhD* value of 1.84 °*C* for sOS01 in the 2098 heatwave. It means that the building configuration (i.e., the combination of passive design strategies) in OS01 leads to the highest risk of overheating in the future. The results also show that the difference in *IOhD* between the three optimal cases increases with worsening heatwave events in the future. In the 2019 heatwave, the *IOhD* difference between OS01 and OS02 is 0.87 °*C*, and it increases up to 1.57 °*C* in the 2098 heatwave. This shows that OS01 will be affected more by intensifying heatwave events due to climate change. This is also confirmed by *CCOR* values for the selected optimal solutions that vary between 4.63 and 21.16. OS01 has the lowest *CCOR* of 4.63, representing the case that will be affected the most by climate change (i.e., least resistant case). On the other hand, OS02 has the highest *CCOR* of 21.16 and therefore

Table 8
Summary of the maximum operative temperature, maximum Heat Index (HI), and Thermal Autonomy (TA) in different zones during the three heatwaves scenarios in OS01, OS02, and OS03.

OS01				
Scenario 01_HW (2019)				
Zone	Office	Living + kitchen	Bedroom 01	Bedroom 02
Max. Op. temperature [°C]	28.19	30.26	28.18	32.86
Max. Heat Index (HI) [°C]	29.29	31.35	29.19	33.61
Thermal autonomy (TA) [%]	36.36	23.10	65.15	24.62
Scenario 02_HW (2047)				
Max. Op. temperature [°C]	29.61	31.75	29.25	34.53
Max. Heat Index (HI) [°C]	29.60	31.31	29.05	33.60
Thermal autonomy (TA) [%]	31.73	26.28	48.07	24.67
Scenario 03_HW (2098)				
Max. Op. temperature [°C]	30.06	33.31	29.83	35.61
Max. Heat Index (HI) [°C]	29.59	32.21	29.20	34.43
Thermal autonomy (TA) [%]	31.71	23.43	38.80	20.31
OS02				
Scenario 01_HW (2019)				
Max. Op. temperature [°C]	28.09	27.03	27.19	26.68
Max. Heat Index (HI) [°C]	29.54	27.94	28.33	27.77
Thermal autonomy (TA) [%]	73.10	84.47	85.60	91.66
Scenario 02_HW (2047)				
Max. Op. temperature [°C]	28.94	27.38	27.72	27.35
Max. Heat Index (HI) [°C]	29.37	28.05	27.97	27.71
Thermal autonomy (TA) [%]	60.89	73.07	78.84	80.12
Scenario 03_HW (2098)				
Max. Op. temperature [°C]	29.35	28.80	28.27	27.95
Max. Heat Index (HI) [°C]	29.19	29.24	28.36	28.63
Thermal autonomy (TA) [%]	62.76	63.80	75	75
OS03				
Scenario 01_HW (2019)				
Max. Op. temperature [°C]	27.36	29.63	28.48	31.27
Max. Heat Index (HI) [°C]	28.63	30.99	28.67	32.34
Thermal autonomy (TA) [%]	71.59	31.81	84.47	40.53
Scenario 02_HW (2047)				
Max. Op. temperature [°C]	28.49	30.85	28.30	32.68
Max. Heat Index (HI) [°C]	28.84	30.80	28.39	32.29
Thermal autonomy (TA) [%]	46.79	28.48	68.91	28.52
Scenario 03_HW (2098)				
Max. Op. temperature [°C]	28.91	32.23	28.83	33.64
Max. Heat Index (HI) [°C]	28.70	31.36	28.90	32.80
Thermal autonomy (TA) [%]	46.61	26.04	65.36	24.74

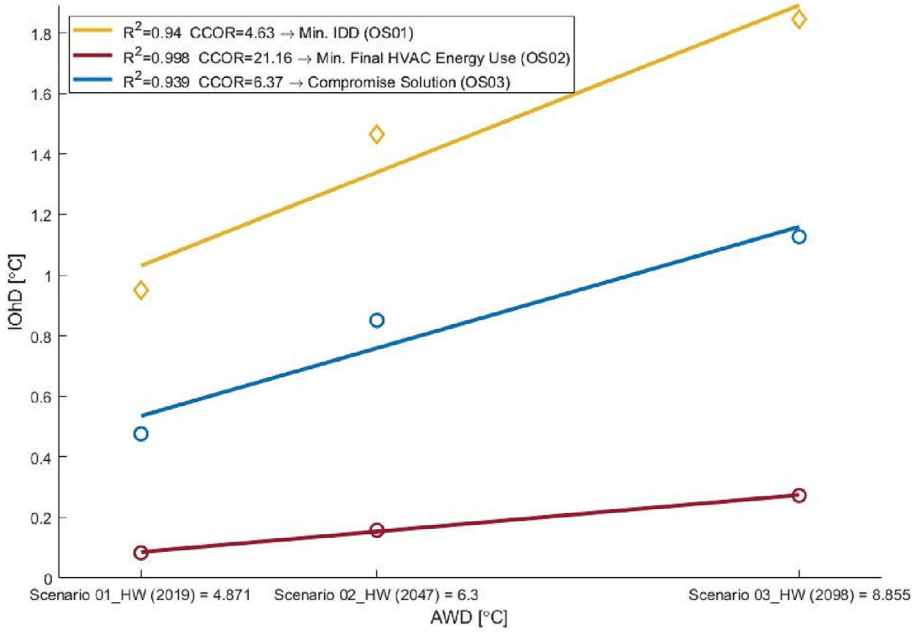

Fig. 10. Indoor Overheating Degree (IOhD) vs. Ambient Warmness Degree (AWD). The inverse of the slope of the regression line shows the Climate Change Overheating Resistivity (CCOR) for each optimal solution.

is the most resistant case. Finally, the relative potential to adapt to climate change P [94] is calculated. P is the difference in $IOhDs$ between optimal solutions in the 2098 heatwave $(\Delta IOhD_{i,j,Scenario03\_HW(2098)})^{+}$ divided by $Max[IOhD_{i,Scenario03\_HW(2098)}, IOhD_{j,Scenario03\_HW(2098)}]$ where i,j = OS01, OS02, or OS03. By calculating P, OS02 shows 83% and 75% more potential to adapt to climate change compared to OS01 and OS03, respectively.

4. Discussion

4.1. Findings and recommendations

According to the Intergovernmental Panel on Climate Change (IPCC), the average global air temperature increased in the past 100 years and will continue to increase due to natural and anthropogenic reasons. The weather data in this paper (derived from MAR BCC-CSM2-MR based on IPCC SSP2-4.5 emission scenario) show an increase in annual mean air temperature 1.4 °C by 2047 and 3.6 °C by 2098 compared to 2019 in Brussels. As illustrated in Fig. 4, the cooling seasons are predicted to extend to shoulder seasons. At the same time, the heating seasons will become warmer and outdoor air temperatures in the range of 15 °C to 18 °C will be experienced more. The $HDD10°C$ will decrease 55% and $CDD18°C$ will increase 148%, shifting Brussels from a heating-dominated region to a cooling-dominated one by the end of the century. In addition, as shown in Fig. 5, the intensity and duration of heatwaves will increase. More severe heatwaves are expected to (i) make it more troublesome for buildings to maintain a thermally safe indoor environment by only relying on passive cooling strategies [119] and (ii) lead to scarcity or failure of the power supply more frequently due to the heavy use of air conditioning [120].

Building design optimization aims to reach energy and cost-effective design with optimum performance in specific circumstances. The combinations of design factors that lead to optimal solutions depend on some parameters, such as climate and building operational properties. In general, to optimize the final HVAC energy use and thermal comfort in any building using passive design strategies, there is a need for making a trade-off between reducing heating energy use/overcooling and cooling energy use/overheating. As shown in Section 3.2, for this specific case study (i.e., nearly Zero-Energy terraced dwelling) and climatic region (i.e., temperate), high ventilation rate, low infiltration rate, high insulation, high thermal mass, integration of green roof, and application of operable roller blinds are found to contribute to both energy efficiency up to 32% and thermal comfort up to 46%. Whilst some factors such as orientation, roof/wall solar absorptance, and Solar Heat Gain Coefficient (SHGC) of windows differ between the best solutions in terms of energy efficiency and thermal comfort. As shown in Table 7, the building orientation towards less exposure to the sun in mostly occupied zones coupled with lower values of wall/roof solar absorptance and windows' SHGC can reduce the cooling energy use, whereas increasing the heating energy use and overcooling discomfort. Differently, the building orientation towards more exposure to the sun in mostly occupied zones coupled with higher values of wall/roof solar absorptance and windows' SHGC can reduce the symmetric thermal discomfort arising mainly from overcooling. Therefore, it works the opposite during the summer and forfeits cooling energy use and summer comfort. This shows that in heating-dominated regions, it is not always the solution to increase solar heat gains to optimize final HVAC energy use and thermal comfort. It is since such a measure may significantly increase the cooling energy use, which can overlap, in some cases, the heating energy use. This is more important considering the impact of climate change and warming weather conditions, which will change the building design concept in temperate regions from heat preserving to heat dissipating to enhance energy efficiency and thermal comfort.

Occupants' exposure to extreme heat in buildings can reach dangerous levels if the mechanical cooling system becomes inoperable. In Fig. 7, Fig. 8, and Fig. 9, it is shown that none of the optimal solutions can fully suppress overheating during concurrent heatwaves and the cooling system outage. The indoor operative temperatures go beyond 29 °C, which can cause serious health issues to the occupants, especially elderly and vulnerable groups. The situation will be aggravated by climate change. By comparing the current and future heatwaves (see Table 8), there is an increase in maximum Heat Index (HI) between 0.28 °C and 0.49 °C, an increase in the maximum operative temperature between 1.34 °C and 2.33 °C, and a decrease in TA between 17% and 28% by 2098 over the three selected optimal solutions. Therefore, provisions are required to increase the preparedness of the buildings against more severe and abnormal conditions to avoid any potential health and comfort issues in the future.

To summarize the main recommendations, the list below is provided:

- It is recommended to analyze the actively heated and cooled buildings not only in normal but also in abnormal conditions such as concurrent heatwave and the outage of the HVAC system. It reveals whether the building can withstand such unprecedented events and keep the indoor environment safe for the occupants.
- Back-up cooling and energy storage systems (e.g., batteries, fuel cells, etc.) should be considered in buildings that fail to maintain a thermally safe environment by only relying on passive measures.
- Due to the continuation of global warming, it is recommended to detach from heat-preserving design concept in temperate regions. The future weather predictions show that such regions will shift from heating-dominated to cooling-dominated ones in the coming decades.
- It is recommended to analyze new buildings and renovations under climate change scenarios to ensure their future performance. It is now imperative that new buildings are designed to be adaptable to a changing climate.
- The use of optimization techniques is recommended during the early design stages of new buildings and the renovation of existing ones. Optimized buildings improve energy, cost, operational efficiency, occupant comfort, and equipment lifecycle [121–123].

4.2. Strengths and limitations

There are numerous methods to conduct scientific research, each with its strengths and limitations. The first strength of the current study is related to the validity of the weather data used for the simulations. As mentioned in Section 2.3, the weather data in this paper are based on the Regional Climate Model (MAR) *"Modèle Atmosphérique Régional"* [68] that has high temporal and spatial resolution (~5 km), detailed parametrization (including mesoscale phenomena), and is tuned for the studied region. In addition, the heatwaves are derived using a statistical method [84], which is adaptable to the studied climate, periods, and geographic region. The second strength of the study relies on the selection of a reference building model as the case study. Therefore, the results are representative and helpful in developing and revising the national or regional building codes. The reference model was developed and validated by some authors of the current paper in a previous study [63]. Third, the paper entails an advanced multi-objective optimization to identify the best combinations of the passive design strategies to enhance energy efficiency and

thermal comfort. Fourth, this paper uses multiple indices to evaluate the overheating risk during heatwaves, including maximum indoor operative temperature, Heat Index (HI), Thermal Autonomy (TA), and Indoor Overheating Degree (IOhD). Such a multi-indicator approach allows to evaluate the building's thermal performance through a more composite, complex, and informative way. Fifth, this paper considers not only current climatic conditions but also future weather projections to analyze the variations in indoor overheating risk due to global warming.

It is plausible that several limitations may have influenced the results obtained. First, the study only assesses three periods (i.e., TMYs for 2010–2020, 2041–2060, and 2081–2100) based on the most likely SSP2-4.5 emission scenario. Therefore, it ignores the intermediate periods (i.e., 2021–2040 and 2061–2080) and other emission scenarios (i.e., SSP1-1.9 "*very low GHG emissions*" and SSP1-2.6 "*low GHG emissions*", SSP3-7.0 "*high GHG emissions*", and SSP5-8.5 "*very high GHG emissions*"). Second, this paper lacks Uncertainty Analysis (UA) and Sensitivity Analysis (SA) to take into account the uncertainties in modelling inputs and to find the most influential factors affecting the final HVAC energy use and thermal comfort. Third, only the indoor operative temperature and relative humidity (latter only in calculating Heat Index "*HI*") are considered while evaluating thermal comfort. However, it is also crucial to consider other comfort factors such as occupant's metabolic rate, clothing insulation, and air velocity. Therefore, more accurate studies are suggested to overcome the limitations of the current paper.

4.3. Implication on practice and future research

The present findings suggest several courses of action to revise current building codes to incorporate compliance criteria during heatwave events. In addition, the new legislation must provide provisions to enhance the preparedness and resistivity of building against global warming. This study also enlightens building professionals, designers, and constructors about the design for climate change. The heat-preserving design concept for buildings in heating-dominated regions should change since it can significantly increase cooling energy use and overheating problems in the future. This study also sheds light on the importance of developing guidelines that include criteria for acute hazard preparation and mitigation strategies as well as chronic risk prevention during abnormal conditions such as power or cooling system outage. Finally, the study establishes a foundation for (IEA) EBC Annex 80 – "Resilient cooling of buildings" project to test and compare different cooling strategies during short-term heatwave events in different climatic zones worldwide. The findings and results will be disseminated publicly to raise awareness about adapting the buildings to such disruptive events.

The findings suggest the following directions for future research. First, future studies should perform similar analyses in other building typologies and climatic regions. In particular, for the Belgian context, the post-World War II buildings are recommended to be studied as the main challenge in renovation schemes [124,125]. Second, further work needs to be carried out by comparing the future weather data obtained from different sources, such as WeatherShift, CORDEX, CCWorldWeatherGen, and Meteonorm. Third, more research is required to improve thermal comfort and overheating indices to incorporate six major comfort parameters (i.e., metabolic rate, clothing factor, relative humidity, air velocity, radiant temperature, and air temperature). Fourth, future research is recommended to perform complementary optimization analyses with different objectives related to cost and environmental impacts. Fifth, the effect of other predicted future global warming scenarios (e.g., SSP1-1.9, SSP1-2.6, SSP3-7.0, and SSP5-8.5) and heatwaves (e.g., the longest and most intense) is of value to be studied in future research. Sixth, further work is recommended to examine the impact of the change of other climate parameters (e.g., wind and humidity) due to climate change on optimal passive design strategies.

5. Conclusion

This paper performs overheating analysis for an optimized nearly Zero-Energy terraced dwelling in Belgium under extreme conditions in two stages. In the first stage, a multi-objective optimization is performed to minimize the final HVAC energy use and thermal discomfort (sum of Indoor Overheating Degree "IOhD" and Indoor Overcooling Degree "IOcD"), considering 13 passive design strategies. In the second stage, three optimal solutions are selected from the resulting Pareto front to analyze the overheating risk during concurrent heatwaves and the cooling system outage. The weather data used in this paper are derived from the Regional Climate Model (MAR) "*Modèle Atmosphérique Régional*". This paper concludes that, i) even under an optimistic emission scenario of SSP2-4.5, the cooling degree days will overlap the heating degree days by the end of the century in a heating-dominated region like Brussels, ii) high ventilation rate, low infiltration rate, high insulation, high thermal mass, integration of green roof, and application of operable roller blinds can be effective in enhancing thermal comfort and energy performance in similar buildings and climates, and iii) overheating in buildings (even in optimized ones) during abnormal conditions such as heatwaves coincided with the cooling system outage can reach critical and unhealthy levels for the occupants. Overall, overheating in buildings is felt and recognized as a major issue arising from climate change in many regions around the world. There is a need today for additional adaptation and provisions to enhance the preparedness of buildings. Multiple effective strategies have been developed so far that can limit the health, productivity, and well-being impacts of overheating. Governments and policymakers can play a critical role in limiting overheating by encouraging proactive adaptation. This can be achieved by establishing a clear path for well-adapted building stock with quantitative targets backed up with appropriate inspection, enforcement, and access to finance [126].

Data availability

Data will be made available on request.

Declaration of Competing Interest

The authors declare that they have no known competing financial interests or personal relationships that could have appeared to influence the work reported in this paper.

Acknowledgments

This research was funded by the Walloon Region under the call 'Actions de Recherche Concertées 2019 (ARC)' (funding number: ARC 19/23-05) and the project OCCuPANt, on the Impacts Of Climate Change on the indoor environmental and energy PerformAnce of buildiNgs in Belgium during summer. The authors would like to gratefully acknowledge the Walloon Region and the University of Liege for funding. We would like to also acknowledge the Sustainable Building Design (SBD) lab at the Faculty of Applied Sciences at the University of Liege for the use of 64-processor workstation during the computation. This study is a part of the International Energy Agency (IEA) EBC Annex 80 – "Resilient cooling of buildings" project activities to define resilient cooling in residential buildings. No potential competing interest was reported by the authors.

References

[1] IPCC WGII core writing team, "Summary for Policymakers: Climate Change 2022 - Impacts, Adaptation, and Vulnerability.," p.7, IPCC Geneva, Switzerland, 2022. Accessed: Jun. 21, 2022. [Online]. Available: https://www.ipcc.ch/report/ar6/wg2/downloads/report/IPCC_AR6_WGII_FinalDraft_FullReport.pdf

[2] S.I. Bohnenstengel, S. Evans, P.A. Clark, S.E. Belcher, Simulations of the London urban heat island, Q. J. R. Meteorol. Soc. 137 (659) (Jul. 2011) 1625–1640, https://doi.org/10.1002/qj.855.

[3] T. Oke, "The heat island of the urban boundary layer: characteristics, causes and effects", *Wind Clim*, Cities (1995) 81–107, https://doi.org/10.1007/978-94-017-3686-2_5.

[4] G. McGregor, "Heatwaves and health: Guidance on warning-system development", World Meterorological Organisation [Online]. Available: World Health Organisation (2015). https://www.who.int/globalchange/publications/heatwaves-health-guidance/en/.

[5] A. Witze, Extreme heatwaves: surprising lessons from the record warmth, Nature 608 (7923) (2022) 464–465, https://doi.org/10.1038/d41586-022-02114-y.

[6] S.J. Brown, Future changes in heatwave severity, duration and frequency due to climate change for the most populous cities, Weather Clim. Extrem. 30 (Dec. 2020), https://doi.org/10.1016/j.wace.2020.100278.

[7] S. Baker, "Europe is battling an unprecedented heat wave, which has set records in 3 countries and is linked to at least 4 deaths," *Business Insider*, Insider Inc., Jul. 25, 2019.

[8] S. Attia, C. Gobin, Climate Change Effects on Belgian Households: A Case Study of a Nearly Zero Energy Building, Energies 13 (20) (2020) 5357, https://doi.org/10.3390/en13205357.

[9] L. Lan, K. Tsuzuki, Y. Liu, Z. Lian, Thermal environment and sleep quality: A review, Energy Build. 149 (2017) 101–113, https://doi.org/10.1016/j.enbuild.2017.05.043Get.

[10] H. Hooyberghs, S. Verbeke, D. Lauwaet, H. Costa, G. Floater, K. De Ridder, Influence of climate change on summer cooling costs and heat stress in urban office buildings, Clim. Change 144 (4) (Oct. 2017) 721–735, https://doi.org/10.1007/s10584-017-2058-1.

[11] HHSRS, "HHSRS Guidance for Landlords and Property-Related Professionals," London, UK, 2006. [Online]. Available: https://www.gov.uk/government/publications/ housing-health-and-safety-rating-system-guidance-for-landlords-and-property-related-professionals

[12] Climate Centre, "European summer heatwaves the most lethal disaster of 2019, says international research group," May 05, 2020. https://www.climatecentre.org/565/european-summer-heatwaves-the-most-lethal-disaster-of-2019-says-international-research-group/ (accessed Jun. 10, 2022).

[13] "In ons land vielen tijdens en vlak na hittegolven 716 doden meer," *De Morgen*, Oct. 03, 2019. Accessed: Jun. 10, 2022. [Online]. Available: https://www.demorgen.be/nieuws/in-ons-land-vielen-tijdens-en-vlak-na-hittegolven-716-doden-meer~b710b9c6/?referrer=https%3A%2F%2Fen.wikipedia.org%2F

[14] Climate Centre, "New official data in Europe exposes heatwaves as still the 'silent killer' of the elderly," Sep. 09, 2019. https://www.climatecentre.org/737/new-official-data-in-europe-exposes-heatwaves-as-still-the-a-silent-killera-of-the-elderly/ (accessed Jun. 10, 2022).

[15] "Heatwave caused nearly 400 more deaths in Netherlands: stats agency," *Reuters*, Aug. 09, 2019. Accessed: Jun. 10, 2022. [Online]. Available: https://www.reuters.com/article/us-weather-netherlands/heatwave-caused-nearly-400-more-deaths-in-netherlands-stats-agency-idUSKCN1UZ0GA?il=0

[16] D. Carrington, "Heatwaves in 2019 led to almost 900 extra deaths in England," *The Guardian*, Jan. 07, 2020. Accessed: Jun. 10, 2022. [Online]. Available: https://www.theguardian.com/world/2020/jan/07/heatwaves-in-2019-led-to-almost-900-extra-deaths-in-england

[17] B. Raddatz, "Almost 500 heat deaths in Berlin last year," Robert Koch Institute, Aug. 29, 2019. Accessed: Jun. 10, 2022. [Online]. Available: https://www.rbb24.de/panorama/thema/2019/klimawandel/beitraege/statistik-hitzetote-sommer-2018-robert-koch-institut.html

[18] A.-T. Nguyen, S. Reiter, P. Rigo, A review on simulation-based optimization methods applied to building performance analysis, Appl. Energy 113 (2014) 1043–1058, https://doi.org/10.1016/j.apenergy.2013.08.061Get, rights and content.

[19] M. Wetter, J. Wright, A comparison of deterministic and probabilistic optimization algorithms for nonsmooth simulation-based optimization, Build. Environ. 39 (8) (2004) 989–999, https://doi.org/10.1016/j.buildenv.2004.01.022.

[20] R. Banos, F. Manzano-Agugliaro, F. Montoya, C. Gil, A. Alcayde, J. Gómez, Optimization methods applied to renewable and sustainable energy: A review, Renew. Sustain. Energy Rev. 15 (4) (2011) 1753–1766, https://doi.org/10.1016/j.rser.2010.12.008.

[21] F. Kheiri, A review on optimization methods applied in energy-efficient building geometry and envelope design, Renew. Sustain. Energy Rev. 92 (Sep. 2018) 897–920, https://doi.org/10.1016/j.rser.2018.04.080.

[22] N. Gunantara, A review of multi-objective optimization: Methods and its applications, Cogent Eng. 5 (1) (2018) 1502242, https://doi.org/10.1080/23311916.2018.1502242.

[23] V. Machairas, A. Tsangrassoulis, K. Axarli, Algorithms for optimization of building design: A review, Renew. Sustain. Energy Rev. 31 (2014) 101–112, https://doi.org/10.1016/j.rser.2013.11.036.

[24] B. Chegari, M. Tabaa, E. Simeu, F. Moutaouakkil, H. Medromi, Multi-objective optimization of building energy performance and indoor thermal comfort by combining artificial neural networks and metaheuristic algorithms, Energy Build. 239 (May 2021), https://doi.org/10.1016/j.enbuild.2021.110839.

[25] A. Vukadinović, J. Radosavljević, A. Đorđević, M. Protić, N. Petrović, Multi-objective optimization of energy performance for a detached residential building with a sunspace using the NSGA-II genetic algorithm, Sol. Energy 224 (Aug. 2021) 1426–1444, https://doi.org/10.1016/j.solener.2021.06.082.

[26] F. Bre, N. Roman, V.D. Fachinotti, An efficient metamodel-based method to carry out multi-objective building performance optimizations, Energy Build. 206 (Jan. 2020), https://doi.org/10.1016/j.enbuild.2019.109576.

[27] S. Gou, V.M. Nik, J.-L. Scartezzini, Q. Zhao, Z. Li, Passive design optimization of newly-built residential buildings in Shanghai for improving indoor thermal comfort while reducing building energy demand, Energy Build. 169 (Jun. 2018) 484–506, https://doi.org/10.1016/j.enbuild.2017.09.095.

[28] K. Li, L. Pan, W. Xue, H. Jiang, and H. Mao, "Multi-Objective Optimization for Energy Performance Improvement of Residential Buildings: A Comparative Study," *Energies*, vol. 10, no. 2, 2017, doi: 10.3390/en10020245.

[29] F. Ascione, N. Bianco, R.F. De Masi, G.M. Mauro, G.P. Vanoli, Design of the Building Envelope: A Novel Multi-Objective Approach for the Optimization of Energy Performance and Thermal Comfort, Sustainability 7 (8) (2015) 10809–10836, https://doi.org/10.3390/su70810809.

[30] F. Ascione, N. Bianco, C. De Stasio, G.M. Mauro, G.P. Vanoli, Simulation-based model predictive control by the multi-objective optimization of building energy performance and thermal comfort, Energy Build. 111 (Jan. 2016) 131–144, https://doi.org/10.1016/j.enbuild.2015.11.033.

[31] W. Yu, B. Li, H. Jia, M. Zhang, D. Wang, Application of multi-objective genetic algorithm to optimize energy efficiency and thermal comfort in building design, Energy Build. 88 (Feb. 2015) 135–143, https://doi.org/10.1016/j.enbuild.2014.11.063.

[32] F. Ascione, N. Bianco, G. Maria Mauro, D.F. Napolitano, Building envelope design: Multi-objective optimization to minimize energy consumption, global cost and thermal discomfort. Application to different Italian climatic zones, Energy 174 (May 2019) 359–374, https://doi.org/10.1016/j.energy.2019.02.182.

[33] A. O' Donovan, M. D. Murphy, and P. D. O'Sullivan, "Passive control strategies for cooling a non-residential nearly zero energy office: Simulated comfort resilience now and in the future," *Energy Build.*, vol. 231, p. 110607, Jan. 2021, doi: 10.1016/j.enbuild.2020.110607.

[34] B. Ozarisoy, Energy effectiveness of passive cooling design strategies to reduce the impact of long-term heatwaves on occupants' thermal comfort in Europe: Climate change and mitigation, J. Clean. Prod. 330 (Jan. 2022), https://doi.org/10.1016/j.jclepro.2021.129675.

[35] A. Laouadi, M. Bartko, M.A. Lacasse, A new methodology of evaluation of overheating in buildings, Energy Build. 226 (Nov. 2020), https://doi.org/10.1016/j.enbuild.2020.110360.

[36] CIBSE TM52, *CIBSE TM52: The limits of thermal comfort: avoiding overheating in European buildings*. Chartered Institution of Building Services Engineers, London, UK: Chartered Institution of Building Services Engineers, London, UK, 2013.

[37] W. Feist, B. Kaufmann, J. Schnieders, O. Kah, Passive house planning package, Passive House Inst. Darmstadt Ger. (2015).

[38] X. Zhou, J. Carmeliet, M. Sulzer, D. Derome, Energy-efficient mitigation measures for improving indoor thermal comfort during heat waves, Appl. Energy 278 (Nov. 2020), https://doi.org/10.1016/j.apenergy.2020.115620.

[39] Y.T. Kwok et al., Thermal comfort and energy performance of public rental housing under typical and near-extreme weather conditions in Hong Kong, Energy Build. 156 (Dec. 2017) 390–403, https://doi.org/10.1016/j.enbuild.2017.09.067.

[40] S.M. Porritt, P.C. Cropper, L. Shao, C.I. Goodier, Ranking of interventions to reduce dwelling overheating during heat waves, Energy Build. 55 (Dec. 2012) 16–27, https://doi.org/10.1016/j.enbuild.2012.01.043.

[41] S. Porritt, L. Shao, P. Cropper, C. Goodier, Adapting dwellings for heat waves, Sustain. Cities Soc. 1 (2) (Jul. 2011) 81–90, https://doi.org/10.1016/j.scs.2011.02.004.

[42] A. Sakka, M. Santamouris, I. Livada, F. Nicol, M. Wilson, On the thermal performance of low income housing during heat waves, Energy Build. 49 (Jun. 2012) 69–77, https://doi.org/10.1016/j.enbuild.2012.01.023.

[43] A. Baniassadi, J. Heusinger, D.J. Sailor, Energy efficiency vs resiliency to extreme heat and power outages: The role of evolving building energy codes, Build. Environ. 139 (Jul. 2018) 86–94, https://doi.org/10.1016/j.buildenv.2018.05.024.

[44] A. Baniassadi, D.J. Sailor, Synergies and trade-offs between energy efficiency and resiliency to extreme heat – A case study, Build. Environ. 132 (Mar. 2018) 263–272, https://doi.org/10.1016/j.buildenv.2018.01.037.

[45] A. Ebrahimi-Moghadam, P. Ildarabadi, K. Aliakbari, F. Fadaee, Sensitivity analysis and multi-objective optimization of energy consumption and thermal comfort by using interior light shelves in residential buildings, Renew. Energy 159 (Oct. 2020) 736–755, https://doi.org/10.1016/j.renene.2020.05.127.

[46] C. Zhang *et al.*, "IEA EBC Annex 80 - Dynamic simulation guideline for the performance testing of resilient cooling strategies: Version 2," Aaalborg University, DCE Technical Reports 306, 2023.

[47] R. Rahif, M. Hamdy, S. Homaei, C. Zhang, P. Holzer, and S. Attia, "Simulation-based framework to evaluate resistivity of cooling strategies in buildings against overheating impact of climate change," *Build. Environ.*, p. 108599, 2022, doi: 10.1016/j.buildenv.2021.108599.
[48] S. Attia et al., "Framework to evaluate the resilience of different cooling technologies", *IEA Annex 80 – Resilient Cool*, Build. (2021), https://doi.org/10.13140/RG.2.2.24588.13447.
[49] D.B. Crawley, J.W. Hand, M. Kummert, B.T. Griffith, Contrasting the capabilities of building energy performance simulation programs, Build. Environ. 43 (4) (2008) 661–673, https://doi.org/10.1016/j.buildenv.2006.10.027.
[50] ANSI/ASHRAE 140-2017, *Standard 140-2017: Standard Method of Test for the Evaluation of Building Energy Analysis Computer Programs*. American Society of Heating, Refrigerating and Air Conditioning Engineers: Atlanta, GA, USA, 2017.
[51] G. Betti, F. Tatarini, S. Schiavon, and C. Nguyen, "CBE Clima Tool. Version 0.4.6.," *Center for the Built Environment, University of California Berkeley*. https://clima.cbe.berkeley.edu (accessed Aug. 19, 2022).
[52] R. Rahif, S. Attia, IOhD (Calculation & illustration), IOcD (Calculation & illustration), AWD (Calculation & illustration), ACD (Calculation & illustration), CCOhR (Calculation), CCOcR (Calculation), Zonal OpT (illustration), and HWs (illustration) v01, Zenodo (Nov. 2022), https://doi.org/10.5281/zenodo.7326901.
[53] R.S. McLeod, M. Swainson, Chronic overheating in low carbon urban developments in a temperate climate, Renew. Sustain. Energy Rev. 74 (Jul. 2017) 201–220, https://doi.org/10.1016/j.rser.2016.09.106.
[54] K.J. Lomas, S.M. Porritt, Overheating in buildings: lessons from research, Build. Res. Inf. (2017), https://doi.org/10.1080/09613218.2017.1256136.
[55] R. Mitchell, S. Natarajan, Overheating risk in Passivhaus dwellings, Build. Serv. Eng. Res. Technol. 40 (4) (2019) 446–469, https://doi.org/10.1177/0143624419842000.
[56] N. Artmann, H. Manz, P. Heiselberg, Parameter study on performance of building cooling by night-time ventilation, Renew. Energy 33 (12) (2008) 2589–2598, https://doi.org/10.1016/j.renene.2008.02.025.
[57] V. Badescu, N. Laaser, R. Crutescu, Warm season cooling requirements for passive buildings in Southeastern Europe (Romania), Energy 35 (8) (2010) 3284–3300, https://doi.org/10.1016/j.energy.2010.04.013.
[58] S.S. Intille, Designing a home of the future, IEEE Pervasive Comput. 1 (2) (2002) 76–82, https://doi.org/10.1109/MPRV.2002.1012340.
[59] S. Phillips, Working through the pandemic: Accelerating the transition to remote working, Bus. Inf. Rev. 37 (3) (2020) 129–134, https://doi.org/10.1177/0266382120953087.
[60] Zero Carbon Hub, Impacts of Overheating: Evidence Review, Zero Carbon Hub, London, England, 2015.
[61] R.S. Kovats, S. Hajat, Heat Stress and Public Health: A Critical Review, Annu. Rev. Public Health 29 (1) (Mar. 2008) 41–55, https://doi.org/10.1146/annurev.publhealth.29.020907.090843.
[62] S. Attia, T. Canonge, M. Popineau, M. Cuchet, Developing a benchmark model for renovated, nearly zero-energy, terraced dwellings, Appl. Energy 306 (Jan. 2022), https://doi.org/10.1016/j.apenergy.2021.118128.
[63] S. Attia, Benchmark model for nearly-zero-energy terraced dwellings, Harv. Dataverse Camb. U. S. (2021), https://doi.org/10.7910/DVN/GJI84W.
[64] R. Rahif et al., Impact of climate change on nearly zero-energy dwelling in temperate climate: Time-integrated discomfort, HVAC energy performance, and GHG emissions, Build. Environ. 223 (Sep. 2022), https://doi.org/10.1016/j.buildenv.2022.109397.
[65] E. Elnagar, A. Zeoli, R. Rahif, S. Attia, V. Lemort, A qualitative assessment of integrated active cooling systems: A review with a focus on system flexibility and climate resilience, Renew. Sustain. Energy Rev. 175 (Apr. 2023), https://doi.org/10.1016/j.rser.2023.113179.
[66] ANSI/ASHRAE Handbook, *Handbook–2017: Fundamentals*. American Society of Heating, Refrigerating and Air Conditioning Engineers: Atlanta, GA, USA, 2017.
[67] V. Pérez-Andreu, C. Aparicio-Fernández, A. Martínez-Ibernón, J.-L. Vivancos, Impact of climate change on heating and cooling energy demand in a residential building in a Mediterranean climate, Energy 165 (Dec. 2018) 63–74, https://doi.org/10.1016/j.energy.2018.09.015.
[68] S. Doutreloup et al., Historical and future weather data for dynamic building simulations in Belgium using the regional climate model MAR: typical and extreme meteorological year and heatwaves, Earth Syst. Sci. Data 14 (7) (2022) 3039–3051, https://doi.org/10.5194/essd-14-3039-2022.
[69] K. De Ridder, H. Gallée, Land surface–induced regional climate change in southern Israel, J. Appl. Meteorol. 37 (11) (1998) 1470–1485, https://doi.org/10.1175/1520-0450(1998)037<1470:LSIRCC>2.0.CO;2.
[70] S. Doutreloup, C. Wyard, C. Amory, C. Kittel, M. Erpicum, X. Fettweis, Sensitivity to convective schemes on precipitation simulated by the regional climate model MAR over Belgium (1987–2017), Atmos. 10 (1) (2019) 34, https://doi.org/10.3390/atmos10010034.
[71] C. Wyard, C. Scholzen, S. Doutreloup, É. Hallot, X. Fettweis, Future evolution of the hydroclimatic conditions favouring floods in the south-east of Belgium by 2100 using a regional climate model, Int. J. Climatol. 41 (1) (2021) 647–662, https://doi.org/10.1002/joc.6642.
[72] H. Hersbach et al., The ERA5 global reanalysis, Q. J. R. Meteorol. Soc. 146 (730) (2020) 1999–2049, https://doi.org/10.1002/qj.3803.
[73] V. Eyring et al., Overview of the Coupled Model Intercomparison Project Phase 6 (CMIP6) experimental design and organization, Geosci. Model Dev. 9 (5) (2016) 1937–1958, https://doi.org/10.5194/gmd-9-1937-2016.
[74] K. Riahi et al., The Shared Socioeconomic Pathways and their energy, land use, and greenhouse gas emissions implications: An overview, Glob. Environ. Change 42 (Jan. 2017) 153–168, https://doi.org/10.1016/j.gloenvcha.2016.05.009.
[75] V. Masson-Delmotte *et al.*, "Climate Change 2021: The Physical Science Basis Contribution of Working Group I to the Sixth Assessment Report of the Intergovernmental Panel on Climate Change," 2021.
[76] R. Pielke Jr, M.G. Burgess, J. Ritchie, Plausible 2005–2050 emissions scenarios project between 2° C and 3° C of warming by 2100, Environ. Res. Lett. 17 (2) (2022), https://doi.org/10.1088/1748-9326/ac4ebf.
[77] R.K. Pachauri et al., Climate change 2014: synthesis report. Contribution of Working Groups I, II and III to the fifth assessment report of the Intergovernmental Panel on Climate Change, Ipcc, 2014.
[78] Global Carbon Project, Supplemental data of Global Carbon Budget 2021 (Version 1.0), Glob. Carbon Proj. 2021 (2021).
[79] L. Cozzi et al., World energy outlook 2020, Int. Energy Agency Paris Fr. (2020) 1–461.
[80] ISO 15927-4, "'ISO 15927-4: Hygrothermal performance of buildings — Calculation and presentation of climatic data — Part 4: Hourly data for assessing the annual energy use for heating and cooling'.," p. Geneva, Switzerland, 2005.
[81] S. Wilcox and W. Marion, "Users Manual for TMY3 Data Sets, Technical report NREL/TP-581-43156, Task No. PVA7.6101," National Renewable Energy Laboratory Golden, CO, 2008. Accessed: Oct. 10, 2022. [Online]. Available: https://www.nrel.gov/docs/fy08osti/43156.pdf, 2008
[82] C.S. Barnaby, U.B. Crawley, Weather data for building performance simulation, Build. Perform. Simul. Des. Oper. (2012) 61–79, https://doi.org/10.4324/9780203891612.
[83] RMI, "Rapport climatique 2020 de l'information aux services climatiques, edited by: Gellens, D., Royal Meteorological Institute of Belgium, Brussels, ISSN 2033-8562," 2020. Accessed: Aug. 31, 2022. [Online]. Available: https://www.meteo.be/resources/misc/climate_report/RapportClimatique-2020.pdf
[84] G. Ouzeau, J.-M. Soubeyroux, M. Schneider, R. Vautard, S. Planton, Heat waves analysis over France in present and future climate: Application of a new method on the EURO-CORDEX ensemble, Clim. Serv. 4 (Dec. 2016) 1–12, https://doi.org/10.1016/j.cliser.2016.09.002.
[85] S. Attia et al., Resilient cooling of buildings to protect against heat waves and power outages: Key concepts and definition, Energy Build. 239 (May 2021), https://doi.org/10.1016/j.enbuild.2021.110869.
[86] K. Deb, A. Pratap, S. Agarwal, T. Meyarivan, A fast and elitist multiobjective genetic algorithm: NSGA-II, IEEE Trans. Evol. Comput. 6 (2) (2002) 182–197, https://doi.org/10.1109/4235.996017.
[87] L. Magnier, F. Haghighat, Multiobjective optimization of building design using TRNSYS simulations, genetic algorithm, and Artificial Neural Network, Build. Environ. 45 (3) (2010) 739–746, https://doi.org/10.1016/j.buildenv.2009.08.016.
[88] F.P. Chantrelle, H. Lahmidi, W. Keilholz, M. El Mankibi, P. Michel, Development of a multicriteria tool for optimizing the renovation of buildings, Appl. Energy 88 (4) (2011) 1386–1394, https://doi.org/10.1016/j.apenergy.2010.10.002.
[89] S. Carlucci, G. Cattarin, F. Causone, L. Pagliano, Multi-objective optimization of a nearly zero-energy building based on thermal and visual discomfort minimization using a non-dominated sorting genetic algorithm (NSGA-II), Energy Build. 104 (2015) 378–394.
[90] J.C. Gamero-Salinas, A. Monge-Barrio, A. Sánchez-Ostiz, Overheating risk assessment of different dwellings during the hottest season of a warm tropical climate, Build. Environ. 171 (Mar. 2020), https://doi.org/10.1016/j.buildenv.2020.106664.
[91] W.A. Mahar, G. Verbeeck, S. Reiter, S. Attia, Sensitivity analysis of passive design strategies for residential buildings in cold semi-arid climates, Sustainability 12 (3) (2020) 1091, https://doi.org/10.3390/su12031091.
[92] J. Mukkavaara, F. Shadram, An integrated optimization and sensitivity analysis approach to support the life cycle energy trade-off in building design, Energy Build. 253 (Dec. 2021), https://doi.org/10.1016/j.enbuild.2021.111529.
[93] K. Menberg, Y. Heo, R. Choudhary, Sensitivity analysis methods for building energy models: Comparing computational costs and extractable information, Energy Build. 133 (Dec. 2016) 433–445, https://doi.org/10.1016/j.enbuild.2016.10.005.
[94] M. Hamdy, S. Carlucci, P.-J. Hoes, J.L.M. Hensen, The impact of climate change on the overheating risk in dwellings—A Dutch case study, Build. Environ. 122 (Sep. 2017) 307–323, https://doi.org/10.1016/j.buildenv.2017.06.031.
[95] R. Rahif, D. Amaripadath, S. Attia, Review on Time-Integrated Overheating Evaluation Methods for Residential Buildings in Temperate Climates of Europe, Energy Build. 252 (Dec. 2021), https://doi.org/10.1016/j.enbuild.2021.111463.
[96] S. Carlucci, L. Pagliano, A review of indices for the long-term evaluation of the general thermal comfort conditions in buildings, Energy Build. 53 (Oct. 2012) 194–205, https://doi.org/10.1016/j.enbuild.2012.06.015.
[97] M. Kazemi, L. Courard, Modelling hygrothermal conditions of unsaturated substrate and drainage layers for the thermal resistance assessment of green roof: Effect of coarse recycled materials, Energy Build. 250 (Nov. 2021), https://doi.org/10.1016/j.enbuild.2021.111315.

[98] RELi 2.0., "Rating Guidelines for Resilient Design + Construction," U.S. Green Building Council, Feb. 2020.
[99] B. Levitt, M. Ubbelohde, G. Loisos, and N. Brown, "Thermal autonomy as metric and design process," presented at the CaGBC National Conference and Expo: Pushing the Boundary-Net Positive Buildings, 2013, pp. 47–58.
[100] L.P. Rothfusz, N.S.R. Headquarters, The heat index equation (or, more than you ever wanted to know about heat index), Ft. Worth Tex. Natl. Ocean. Atmospheric Adm. Natl. Weather Serv. Off. Meteorol. 9023 (1990).
[101] M. Zune, L. Rodrigues, M. Gillott, The vulnerability of homes to overheating in Myanmar today and in the future: A heat index analysis of measured and simulated data, Energy Build. 223 (2020), https://doi.org/10.1016/j.enbuild.2020.110201.
[102] A.R. Rempel, J. Danis, A.W. Rempel, M. Fowler, S. Mishra, Improving the passive survivability of residential buildings during extreme heat events in the Pacific Northwest, Appl. Energy 321 (Sep. 2022), https://doi.org/10.1016/j.apenergy.2022.119323.
[103] E.S. Quigley, K. Lomas, "Performance of medium-rise, thermally lightweight apartment buildings during a heat wave", presented at the Proceedings of 10th Windsor Conference: Rethinking Comfort, London, UK, Apr, Windsor, 2018, pp. 32–47.
[104] K. Sun, M. Specian, T. Hong, Nexus of thermal resilience and energy efficiency in buildings: A case study of a nursing home, Build. Environ. 177 (Jun. 2020), https://doi.org/10.1016/j.buildenv.2020.106842.
[105] K. Papakostas, N. Kyriakis, Heating and cooling degree-hours for Athens and Thessaloniki, Greece, Renew. Energy 30 (12) (2005) 1873–1880, https://doi.org/10.1016/j.renene.2004.12.002.
[106] D.J. Sailor, Relating residential and commercial sector electricity loads to climate—evaluating state level sensitivities and vulnerabilities, Energy 26 (7) (Jul. 2001) 645–657, https://doi.org/10.1016/S0360-5442(01)00023-8.
[107] A. Ploskić, Q. Wang, Evaluating the potential of reducing peak heating load of a multi-family house using novel heat recovery system, Appl. Therm. Eng. 130 (Feb. 2018) 1182–1190, https://doi.org/10.1016/j.applthermaleng.2017.11.072.
[108] R. Rahif A. Fani S. Attia Climate Change Sensitive Overheating Assessment in Dwellings: A Case Study in Belgium Proceeding of the International Building Simulation Conference 2021 Bruges, Belgium 30125 30131 [Online]. Available:
[109] R. Becker, I. Goldberger, M. Paciuk, Improving energy performance of school buildings while ensuring indoor air quality ventilation, Build. Environ. 42 (9) (2007) 3261–3276, https://doi.org/10.1016/j.buildenv.2006.08.016.
[110] M. Gil-Baez, Á. Barrios-Padura, M. Molina-Huelva, R. Chacartegui, Natural ventilation systems in 21st-century for near zero energy school buildings, Energy 137 (2017) 1186–1200, https://doi.org/10.1016/j.energy.2017.05.188.
[111] E. Tavakoli, A. O'Donovan, M. Kolokotroni, P.D. O'Sullivan, Evaluating the indoor thermal resilience of ventilative cooling in non-residential low energy buildings: A review, Build. Environ. 222 (Aug. 2022), https://doi.org/10.1016/j.buildenv.2022.109376.
[112] K. Hassouneh, A. Alshboul, A. Al-Salaymeh, Influence of infiltration on the energy losses in residential buildings in Amman, Sustain. Cities Soc. 5 (2012) 2–7, https://doi.org/10.1016/j.scs.2012.09.004.
[113] U. Mathur, R. Damle, Impact of air infiltration rate on the thermal transmittance value of building envelope, J. Build. Eng. 40 (Aug. 2021), https://doi.org/10.1016/j.jobe.2021.102302.
[114] J. Jokisalo, J. Kurnitski, M. Korpi, T. Kalamees, J. Vinha, Building leakage, infiltration, and energy performance analyses for Finnish detached houses, Build. Environ. 44 (2) (2009) 377–387, https://doi.org/10.1016/j.buildenv.2008.03.014.
[115] J. Lee, J. Kim, D. Song, J. Kim, C. Jang, Impact of external insulation and internal thermal density upon energy consumption of buildings in a temperate climate with four distinct seasons, Renew. Sustain. Energy Rev. 75 (Aug. 2017) 1081–1088, https://doi.org/10.1016/j.rser.2016.11.087.
[116] S.A. Al-Sanea, M.F. Zedan, S.N. Al-Hussain, Effect of thermal mass on performance of insulated building walls and the concept of energy savings potential, Spec. Issue Therm. Energy Manag. Process Ind. 89 (1) (Jan. 2012) 430–442, https://doi.org/10.1016/j.apenergy.2011.08.009.
[117] J. Goussous, H. Siam, H. Alzoubi, Prospects of green roof technology for energy and thermal benefits in buildings: Case of Jordan, Sustain. Cities Soc. 14 (Feb. 2015) 425–440, https://doi.org/10.1016/j.scs.2014.05.012.
[118] A. Sfakianaki, E. Pagalou, K. Pavlou, M. Santamouris, M. Assimakopoulos, Theoretical and experimental analysis of the thermal behaviour of a green roof system installed in two residential buildings in Athens, Greece, Int. J. Energy Res. 33 (12) (2009) 1059–1069, https://doi.org/10.1002/er.1535.
[119] B. Stone et al., Climate change and infrastructure risk: Indoor heat exposure during a concurrent heat wave and blackout event in Phoenix, Arizona, Urban Clim. 36 (Mar. 2021), https://doi.org/10.1016/j.uclim.2021.100787.
[120] B. Stone Jr et al., Compound climate and infrastructure events: how electrical grid failure alters heat wave risk, Environ. Sci. Technol. 55 (10) (2021) 6957–6964, https://doi.org/10.1021/acs.est.1c00024.
[121] M. Hamdy, K. Sirén, S. Attia, Impact of financial assumptions on the cost optimality towards nearly zero energy buildings – A case study, Energy Build. 153 (Oct. 2017) 421–438, https://doi.org/10.1016/j.enbuild.2017.08.018.
[122] T. Hong, Z. Wang, X. Luo, W. Zhang, State-of-the-art on research and applications of machine learning in the building life cycle, Energy Build. 212 (Apr. 2020), https://doi.org/10.1016/j.enbuild.2020.109831.
[123] M. Ferrara, E. Fabrizio, J. Virgone, M. Filippi, Energy systems in cost-optimized design of nearly zero-energy buildings, Autom. Constr. 70 (2016) 109–127, https://doi.org/10.1016/j.autcon.2016.06.007.
[124] G. Ruellan, M. Cools, S. Attia, Analysis of the determining factors for the renovation of the Walloon residential building stock, Sustainability 13 (4) (2021) 2221, https://doi.org/10.3390/su13042221.
[125] S. Attia, A. Mustafa, N. Gir1y, M. Popineau, M. Cuchet, N. Gulirmak, Developing two benchmark models for post-world war II residential buildings, Energy Build. 244 (Aug. 2021), https://doi.org/10.1016/j.enbuild.2021.111052.
[126] T. Dooks, "Risks to health, wellbeing and productivity from overheating in buildings," *Clim. Change Comm.*, Jul. 2022, Accessed: Oct. 10, 2022. [Online]. Available: https://www.theccc.org.uk/publication/risks-to-health-wellbeing-and-productivity-from-overheating-in-buildings/